Chapter 5

Soil micromorphology, loss-on-ignition, phosphate-P concentrations and magnetic susceptibility analyses

by Richard Macphail, John Crowther and Francis Wenban-Smith

INTRODUCTION

A range of sediment analytical techniques was applied to help understand formation processes associated with the main archaeological horizons, and to perhaps explain some of the apparent stratigraphic breaks and discolorations in the sequence. Analysis was mostly focused on sediments from Phase 6, which contained the richest archaeological remains, including the elephant skeleton and the flint concentration south of Trench D, but also included investigation of the Phase 1 sequence in the 'Tilted Block'. A selection of 16 monoliths was initially examined (Fig. 5.1), leading to identification of 19 target areas for thin section sediment micromorphology, which was complemented by analysis of 'loss-on-ignition' (LOI) and Phosphate-P for 12 associated bulk samples (Table 5.1).

This work was subsequently reinforced by much more detailed LOI and magnetic susceptibility (χ) analyses of 79 more closely spaced samples through the same sequences (Table 5.2), in the hope of identifying soils and/or palaeo-landsurfaces. As the sediments accumulated, it would be anticipated that former soils/land surfaces would have had a relatively high organic matter content (as estimated by LOI) as a result of plant growth and inputs of organic litter. An enhanced magnetic susceptibility would also be anticipated as a consequence of natural fermentation processes within soils (Le Borgne 1955). It should be noted, however, that both properties may have been significantly affected by post-depositional processes. Organic matter content is likely to have diminished as a result of decomposition processes and magnetic susceptibility may have been affected by the mobilisation (through gleying), leaching and reprecipitation of iron (Fe) compounds as a result of waterlogging. Also, magnetic susceptibility is affected both by the degree of enhancement and the Fe content, and where (as is likely to be the case in these sedimentary sequences) the latter is quite variable then may poorly reflect the levels of enhancement. The LOI and χ data therefore need to be interpreted with caution.

SAMPLES AND METHODS

Loss-on-ignition (LOI) and phosphate-P

Loss-on-ignition (LOI) and phosphate-P analysis was undertaken on the fine earth fraction (ie < 2 mm) of the bulk samples. LOI was determined by ignition at 375^{o}C for 16 hrs (Ball 1964). Phosphate-P concentrations were determined colorimetrically following alkaline oxidation with NaOBr, using NH_2SO_4 as extractant (Dick and Tabatabai 1977).

A broad overview of the analytical data from the initial selection of bulk samples, with key features relating to individual contexts highlighted, is presented here (Table 5.3). Full results from more detailed analyses through the different sequences studied are given as an appendix (Appendix 2); significant results from key parts of the site sequence are presented below, in conjunction with the thin section analyses from different parts of the site sequence. All the samples analysed are largely minerogenic; nine of the initial samples have LOI values of < 3.00%; two (both from 40100) have a somewhat higher LOI of 3.42 and 3.63%; and one (from 40158) has a much higher LOI (6.68%). It should also be noted that a number of samples which appeared (by virtue of their darker colour) to be more organic, did not necessarily have relatively high LOI values. LOI in these predominantly minerogenic sediments may be picking up the influence of textural variations between different contexts, with finer-textured contexts having a generally higher LOI. In interpreting these data it should also be borne in mind that organic matter in the various contexts will have been subject to post-depositional decomposition, in other words the LOI recorded therefore underestimates the original organic matter content. The two samples with somewhat higher LOI values may therefore be potentially quite significant within the sequence, perhaps representing periods of soil development. Indeed, the sample from context 40158 could well be derived from what was originally quite a humic, possibly peaty, deposit (see below).

The phosphate-P concentrations exhibit quite marked variability (range: 0.124–1.77mg g^{-1}), though nine of the samples have low concentrations of ≤ 0.346 mg g^{-1}. Somewhat surprisingly, the most organic-rich sample (from context 40158) has the lowest phosphate-P concentration. This is certainly counter-intuitive and tends to suggest that there has been significant post-depositional depletion and movement of phosphate within the sequence. Such movement within the permanently or temporarily waterlogged deposits could be associated with the mobilisation, leaching and deposition of iron. Such a process would seem to be supported

Table 5.1 Overview of source monoliths for thin sections and initial LOI and Phosphate-P bulk samples

Site provenance Site area	Section	Monolith no. <>	Phase	Thin section no.	Depth (cm)	Context/s	Bulk sample no.	Depth (cm)	Context
Central (N)	40091	40418	7/6	M40418A	4.5-12.5	40166/40158	-	-	-
			6	M40418A	7-11(11-12.5)	40158	x40158	7-9	40158
			6/6a	M40418B	17-25	40158/40040	-	-	-
			6a-5	M40418C	40-45	40040-40025	-	-	-
			6-6a-5	M40418C	45-48	40158-40040-40025	-	-	-
Central (El)	40015	40149	6	M40149	35-43	40078-40099	x40099	30-35	40099, brownish
Central (El)	40015	40150	6	M40150A	22-24(27)	40099	-	-	-
			6/6a	M40150A	24(27)-38	40099/40103	x40103-Fe pan	24-25	40099/40103 boundary
			6a	M40150B	22-38	40103	x40103-Fe mottling	33-35	40103
Central (El)	40015	40151	6a	M40151A	7-15	40103/40039	-	-	-
			6a/5	M40151B	32-41	40039/40025	x40039	35-38	40039
Central (El)	40085	40365	6	M40365A	5-13	40078/40099	x40078	5-7	40078
			6	M40365B	22-30	40099, brownish	x40099	28-30	40099, brownish
			6	M40365C	31-39	40099, brownish	-		
Central (E)	40082	40323	6a	M40323A	0-7	40039	-	-	-
			6a	M40323B	7-13	40039	-	-	-
South (W)	40015 (S end)	40196	6	M40196	8.5-16.5	40100	x40100-a	10-16	40100, brownish
							x40100-b	10-16	40100, greyish
South (W)	40015 (S end)	40195	6	M40195	13-21	40100 (sandy lenses)	-	-	-
South (W)	40015 (S end)	40194	6	M40194	32-40	40100 (stones/artefact inclusions?)		-	- -
South (W)	40015 (S end)	40193	6/6a	M40193A	29-37	40100/40039	40039-top	30-32	40039, top part, strongly mottled
							40039	34-38	40039
			6a	M40193B	37-45	40039	-	-	-
South (E)	40016	40082	1	M40082	29-37	40057	x40057	35-37	40057

Table 5.2 Expanded LOI and magnetic susceptibility (χ) sampling through selected sequences

Figs 5.1 and 5.2 reference	*Phase*	*Context*	*Monolith* <>	*Sampling depth (cm)*	*Sequence depth (cm)*	*Notes*
(f)	7	40166	40418	2-3	2.5	
	6	40158	40418	12-13	12.5	
	6	40158	40418	25-26	25.5	
	6a	40040	40418	36-37	36.5	Stratigraphy complex here; 40160 used for fine yellowish-brown sand wedging out to W, thickening and interdigitating to E with Phase 5
	6a/5	40160	40419	4-5	43	
	6	40158	40418	44-45	44.5	Stratigraphy complex here; 40160 used for fine yellowish-brown sand wedging out to W, thickening and interdigitating to E
	6	40158	40419	11-12	50	Context 40158 (here, in Section 40091, Trench B) is equivalent to the particularly dark facies of 40039 in the central part of the main west facing section in the vicinity of Log 40011
	6	40158	40419	21-22	60	
	6a	40040	40419	31-32	70	
	5	40025	40419	42-43	81	Transitional to 40025
(e)	6	40100	40148	4-5	4.5	
	6	40100	40148	11-12	11.5	
	6	40078	40148	21-22	21.5	
	6	40078	40148	30-31	30.5	
	6	40078	40148	43-44	43.5	
	6	40078	40149	15-16	40.5	
	6	40078	40149	22-23	47.5	
	6	40078	40149	32-33	57.5	
	6	40099	40149	44-45	69.5	
	6	40099	40150	7-8	77.5	
	6	40099	40150	17-18	87.5	Overlap
	6a	40103	40150	32-33	102.5	
	6a	40103	40150	42-43	112.5	
	6a	40039	40151	8-9	111	
	6a	40039	40151	17-18	120	
	6a	40039	40151	24-25	127	
	6a	40039	40151	34-35	137	
	6a	40039	40151	44-45	147	
	5	40025	40152	8-9	148.5	
	5	40025	40152	15-16	155.5	
	5	40025	40152	24-25	164.5	
	5	40025	40152	33-34	173.5	
	5	40025	40152	43-44	183.5	
(d)	6	40078	40365	4-5	4.5	
	6	40099	40365	9-10	9.5	
	6	40099	40365	15-16	15.5	
	6	40099	40365	23-24	23.5	
	6a	40099	40365	30-31	30.5	
	6a	40103	40365	40-41	40.5	
	6a	40103	40365	50-51	50.5	
(c)	6b	40070	40322	4-5	4.5	
	6a	40103	40322	11-12	11.5	
	6a	40039	40323	2-3	22.5	
	6a	40039	40323	11-12	31.5	

continued overleaf

Table 5.2 (continued)

Figs 5.1 and 5.2 reference	*Phase*	*Context*	*Monolith <>*	*Sampling depth (cm)*	*Sequence depth (cm)*	*Notes*
(b)	6	40100	40196	4-5	4.5	
	6	40100	40196	14-15	14.5	
	6	40100	40196	24-25	24.5	
	6	40100	40196	34-35	34.5	
	6	40100	40196	44-45	44.5	
	6	40100	40195	6-7	44	
	6	40100	40195	16-17	54.0	
	6	40100	40195	26-27	64.0	
	6	40100	40195	36-37	74.0	
	6	40100	40195	46-47	84.0	
	6	40100	40194	6-7	81.5	
	6	40100	40194	9-10	84.5	
	6	40100	40194	16-17	91.5	
	6	40100	40194	26-27	101.5	
	6	40100	40194	36-37	111.5	
	6	40100	40194	46-47	121.5	
	6	40100	40193	7-8	122.5	
	6	40100	40193	17-18	132.5	
	6	40100	40193	27-28	142.5	
	6	40039	40193	37-38	152.5	
	6	40039	40193	47-48	162.5	Transitional from context 40039 to 40025?
(a)	1	40058	40082	8-9	8.5	
	1	40058	40082	18-19	18.5	
	1	40058	40082	28-29	28.5	
	1	40057	40082	38-39	38.5	
	1	40057	40082	51-52	51.5	
	1	40057	40081	5-6	5.5	
	1	40057	40081	8-9	8.5	
	1	40057	40081	15-16	15.5	
	1	40057	40081	18-19	18.5	
	1	40057	40081	25-26	25.5	
	1	40056	40081	28-29	28.5	
	1	40056	40081	35-36	35.5	
	1	40056	40081	38-39	38.5	
	1	40056	40081	45-46	45.5	
	1	40056	40081	48-49	48.5	

Table 5.3 Analytical data from bulk samples

Phase	*Context*	*Bulk sample no. <>*	*Thin section*	*Bulk sample depth (cm)*	*LOI -%*	*Phosphate P (mg g^{-1})*
6	40158	x40158	M40418A	7-9	6.68**	0.124
6	40099, brownish	x40099	M40149	30-35	2.16	0.194
6/6a	40099/40103 boundary	x40103-Fe pan	M40150A	24-25	3.63*	1.77**
6a	40103	x40103-Fe mottling	M40150B	33-35	3.42*	0.538*
6a	40039	x40039	M40151B	35-38	1.88	0.556*
6	40078	x40078	M40365A	5-7	2.44	0.226
	40099, brownish	x40099	M40365B	28-30	2.57	0.346
6	40100, brownish	x40100-a	M40196	10-16	2.52	0.276
	40100, greyish	x40100-b		10-16	1.9	0.127
6a	x40039, strong Fe mottles	40039-top	M40193A	30-32	1.69	0.15
	x40039, Fe mottles	40039		34-38	1.73	0.179
1	40057	x40057	M40082	35-37	1.22	0.156

LOI: samples all largely minerogenic, higher values are highlighted (* = 2.50–4.99%, ** ≥5.00%) Phosphate-P: samples showing likely signs of enrichment are highlighted (* = slightly enriched 0.500–0.999 mg/g^{-1}), ** = enriched 1.00–1.99 mg/g^{-1})

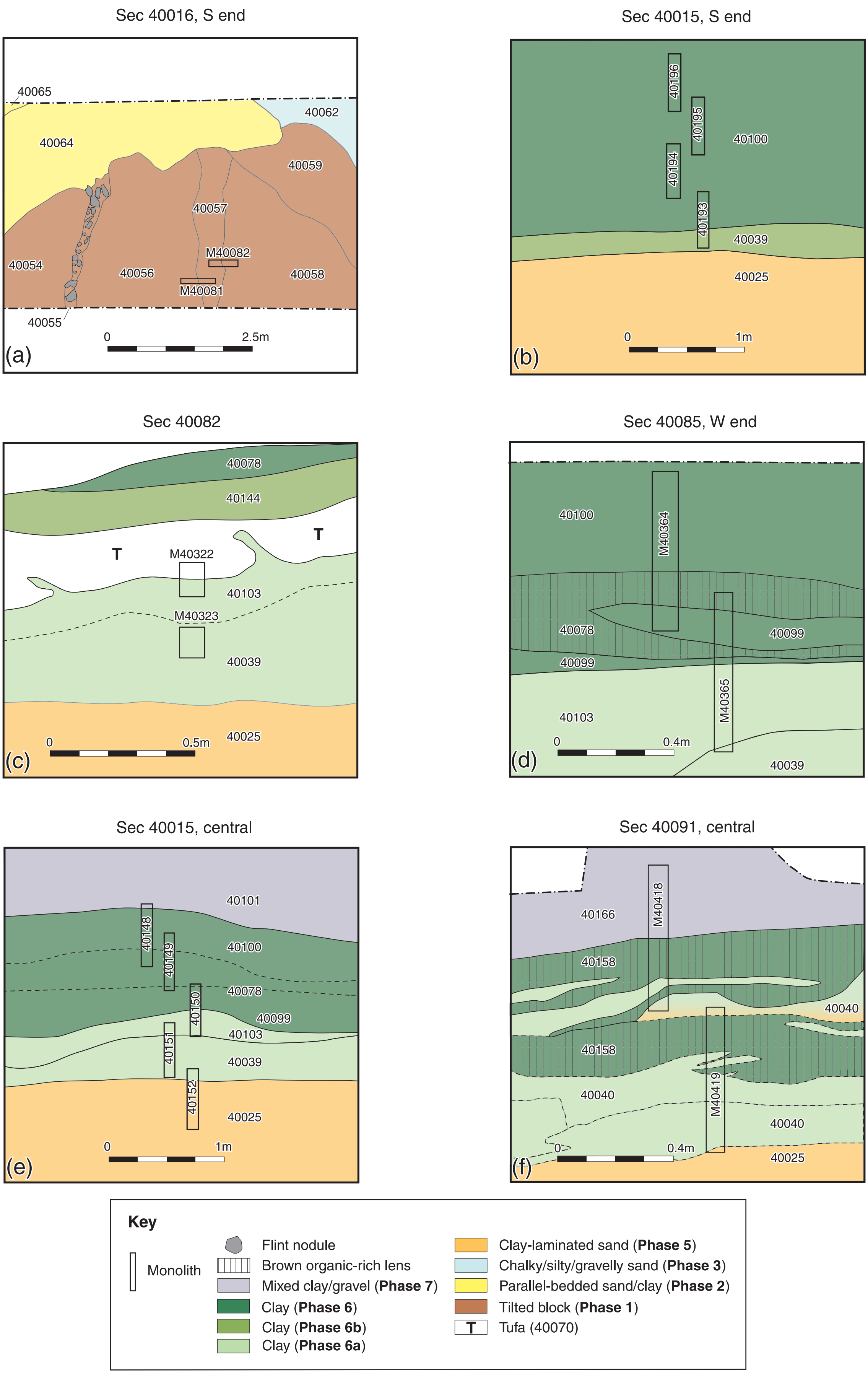

Figure 5.1 Locations of analysed monoliths within local stratigraphic sequences: (a) Phase 1, 'Tilted block'; (b) Phase 6/6a, south of Trench D (west side of site); (c) Phase 6b/6a, tufaceous channel (central east side of site); (d) Phase 6/6a, west end of Trench C, near elephant; (e) Phase 6/6a/5, central west side of site, near elephant; and (f) Phase 7/6/6a, north side of Trench B, central part of site

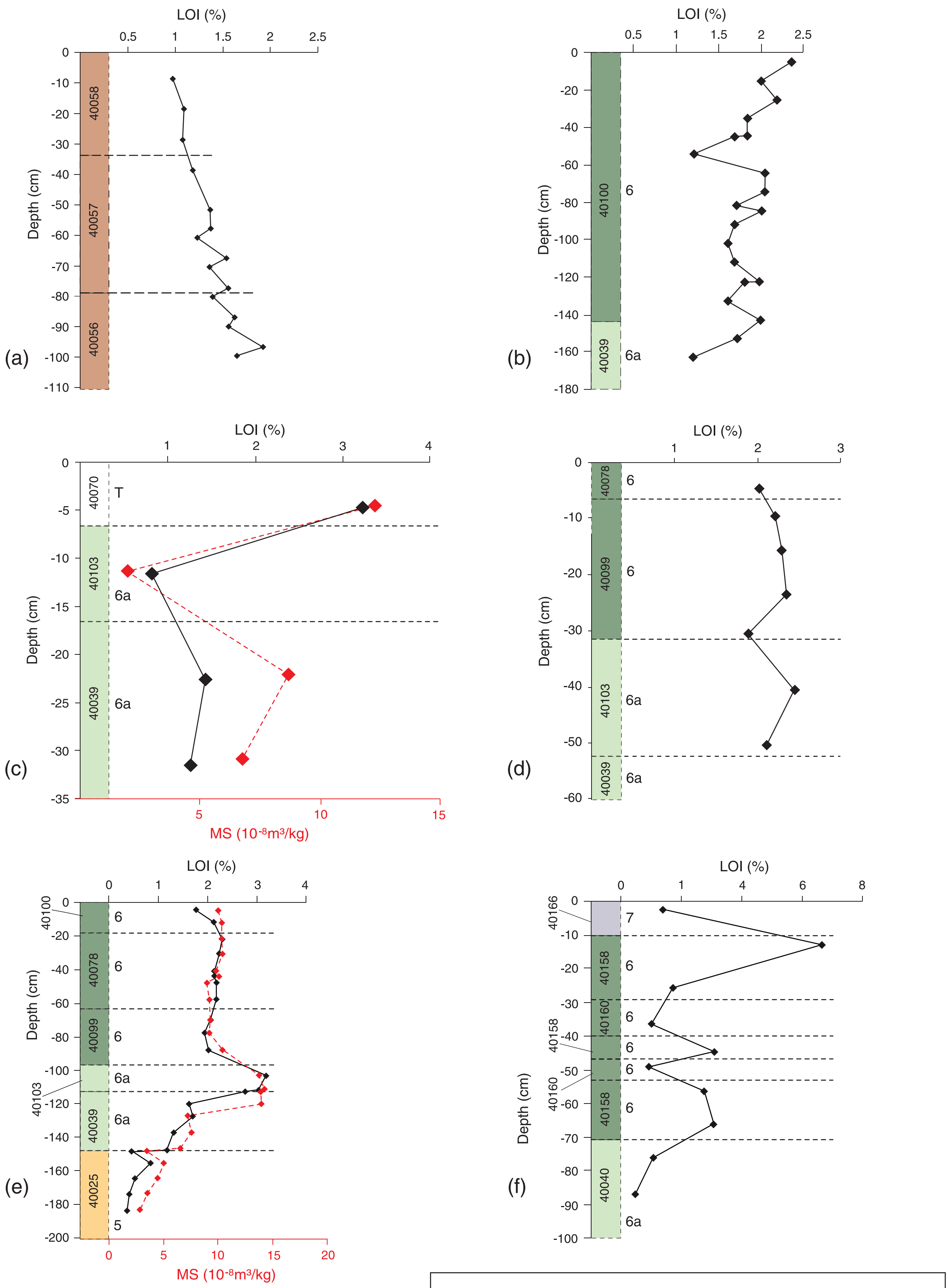

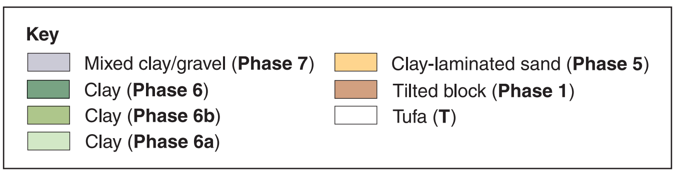

Figure 5.2 Variations in LOI (%) and magnetic susceptibility (χ) through analysed sequences shown in Fig. 5.1: (a) Phase 1, 'Tilted block' through monoliths <40082> and <40081>; (b) Phase 6/6a, south of Trench D (west side of site) through monoliths <40196-40193>; (c) Phase 6b/6a, tufaceous channel (central east side of site) through monoliths <40322> and <40323>; (d) Phase 6/6a, west end of Trench C, near elephant through monolith <40365>; (e) Phase 6/6a/5, central west side of site, near elephant through monoliths <40148> and <40152>; and (f) Phase 7/6/6a, north side of Trench B, central part of site, through monoliths <40418> and <40419>

by the fact that the highest concentration (1.77mg g^{-1}) occurs in the Fe-pan of the sample from context 40103 (discussed further below). In these circumstances, variations in phosphate-P concentrations through the sequence are more likely to reflect patterns of post-depositional redistribution than the original phosphate content of individual contexts, so little further reference is made to the phosphate-P data below.

Magnetic susceptibility (χ)

In addition to χ, determinations were made of χ_{max} (maximum potential magnetic susceptibility, which generally closely reflects the iron content) on 20 samples, representative of the range of χ values recorded, by subjecting a sample to optimum conditions for susceptibility enhancement in the laboratory. χ_{conv} (fractional conversion), which is expressed as a percentage, is a measure of the extent to which the potential susceptibility has been achieved in the original sample, viz: (χ/χ_{max}) x 100.0 (Tite 1972; Scollar *et al.* 1990). In many respects this is a better indicator of magnetic susceptibility enhancement than raw data, particularly in cases where sediments have widely differing χ_{max} values (Crowther and Barker 1995; Crowther 2003). A Bartington MS2 meter was used for magnetic susceptibility measurements. χ_{max} was achieved by heating samples at 650°C in reducing, followed by oxidising conditions. The method used broadly follows that of Tite and Mullins (1971), except that household flour was mixed with the soils and

Table 5.4 Thin section SEM/EDS analyses: (a): M40151B, see Fig. 5.3a, Fig. 5.4a and Fig. 5.13; and (b) M40150A, see Fig. 5.3b and Fig. 5.4b (%; analysed areas and spots)

	Mg	*Al*	*Si*	*P*	*K*	*Ca*	*Ti*	*Fe*
Area 1								
Matrix	0.93	10.9	31.8		1.73	1.07	0.73	3.90
Fe-staining	0.82	8.18	17.2		1.46	0.55	0.98	32.8
Fe-P-staining 1		6.23	12.5	0.65	0.60	0.53	0.90	43.7
Fe-P- staining 2	0.84	7.43	12.1	0.76	1.01	0.83	0.65	41.6
Fe-P- staining 3	1.16	9.95	21.0	0.55	1.47	0.79	0.73	22.5
Area 2								
Void coating	1.63	7.08	31.0		3.59	0.75		9.54
Matrix	1.16	10.9	31.4		2.39	0.84	0.66	3.98
Pale infill	1.37	16.0	25.0		8.18		0.55	2.41
Area 3								
Fe-P-nodule 1		1.71	10.4	1.07		0.57		55.3
Fe-P-nodule 2		3.82	4.86	1.10		0.86		61.1
Fe-P-nodule 3	0.93	7.09	14.4	0.97	1.05	0.71		38.7
Fe-P-nodule 4		1.86	2.76	1.33		0.85		67.1
Fe-P-staining		5.71	9.81	1.04	0.70	0.76	0.65	48.9
Fe-staining	1.13	20.2	20.8		2.10	0.84		23.8
Fe-void hypocoating	1.04	9.88	26.6		2.07	1.07	0.51	13.8
Matrix	1.37	11.5	25.7		2.35	0.78	0.56	12.7
Pale infill	1.23	12.1	29.9		2.61	0.92	0.60	4.43

(a) M40151B

	Mg	*Al*	*Si*	*P*	*K*	*Ca*	*Ti*	*Fe*
Area 1 Iron pan 40103								
Marked iron impregnated sediment	0.79	6.74	15.9	1.35	1.12	1.01	0.33	35.4
Ditto	0.47	5.69	11.3	1.75	0.70	1.09	0.29	44.6
Background matrix	1.26	10.6	25.8	0.37	2.22	1.04	0.40	13.2
Area 2 Overlying depleted sediment 40099								
Sediment	1.06	11.4	29.8		2.34	0.99	0.75	5.80
Ditto	1.45	11.9	29.5		2.58	0.93	0.63	5.02
Area 3 Iron pan								
Marked iron impregnated sediment	0.62	6.34	13.9	1.35	1.00	0.84	0.36	39.8
Ditto	0.41	8.12	8.50	1.29	0.80	0.92	0.08	47.0
Background matrix	1.33	10.8	26.8	0.19	2.34	0.83	0.65	11.4
Area 4 Iron pan 40103								
Iron void hypocoating	0.78	5.99	10.8	1.25	1.06	0.99	0.33	45.2
Area 5 Overlying depleted sediment 40099								
Sediment	1.13	12.3	29.5		2.19	0.88	0.55	5.32

(b) M40150A

lids placed on the crucibles to create the reducing environment (after Graham and Scollar 1976; Crowther and Barker 1995).

The most striking feature of the magnetic susceptibility data was the extremely high variability in χ_{max} with values ranging from 22.0–7390 x 10^{-8} m^3 kg^{-1} (Appendix 2). Given this exceptionally high variability, and the relatively low variability in χ (range, 2.0–27.4 x 10^{-8} m^3 kg^{-1}), it is highly unlikely that there will be a strong relationship between χ and χ_{conv} (Crowther 2003). Furthermore, since such variability in χ_{max} is likely to be largely attributable to variations in Fe content, which in these sedimentary sequences could well have been subject to post-depositional change through gleying and associated

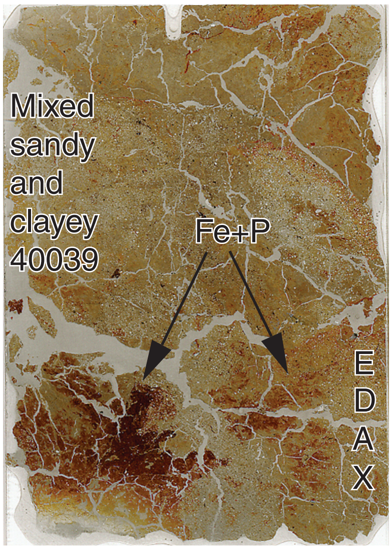

(a): Scan of M40151B, showing mixing of clayey and coarse silt-fine sandy microfacies, location of ferruginised, earlier-formed wood(?) peat, and iron (and phosphate) staining - this and mixing perhaps related to large animal trampling (see Figs 5.13(a)-(h)); note SEM/EDS study area (see T5.4 and Figs 5.13(g)-(h) and Fig 5.4a). Width is ~50mm.

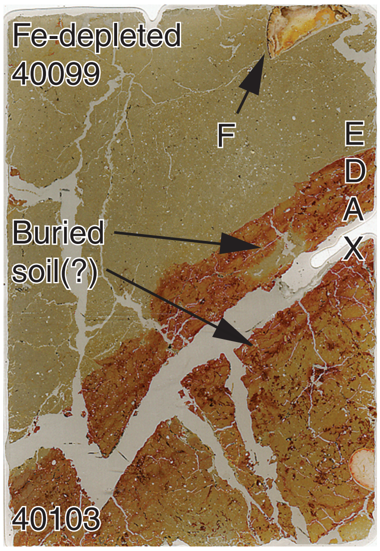

(b): Scan of M40150A; junction of buried soil (upper 40103) and inundation clay (lower 40099); flint (F) and SEM/EDS study are located (see Table 5.4 and Fig 5.4(b)).

(c) Scan of M40196 (Context 40100), showing greyish and brownish microfacies types; three flint flakes occur in the uppermost layer. Width is ~50mm.

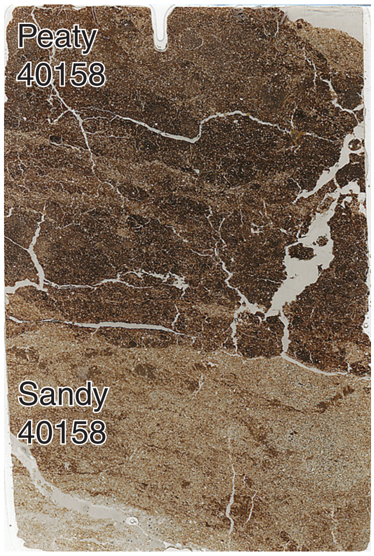

(d): Scan of M40418B showing sandy and peaty microfacies variants in Context 40158 (see Figs 5.19(a)-(d)).

Figure 5.3 Thin Sections after polishing: (a)–(d) leaching/reprecipitation, the χ and χ_{max} data may poorly reflect the characteristics of the sediments at the time of deposition. Thus, little reliance can be placed on the magnetic susceptibility data, with samples with a high χ_{conv} (maximum, 37.7%) not necessarily being indicative of significant enhancement in the original sediments. Therefore, although the full analyses are presented in Appendix 2, little reference to the magnetic susceptibility data is made in the discussion below.

Soil micromorphology and SEM/EDS analysis

The nineteen thin section subsamples (designated Mxxx, based on the monolith sample number <xxx>) were impregnated with a clear polyester resin-acetone mixture; samples were then topped up with resin, ahead of curing and slabbing for 75x50mm-size thin section manufacture by Spectrum Petrographics, Vancouver, Washington, USA (Goldberg and Macphail 2006; Murphy 1986). Thin sections were further polished with 1,000 grit papers (Fig. 5.3) and analysed using a petrological microscope under plane polarised light (PPL), crossed polarised light (XPL), oblique incident light (OIL) and using fluorescent microscopy (blue light – BL), at magnifications ranging from x1 to x200/400. Thin sections M40150A and M40151B were also analysed employing quantitative SEM/EDS analyses (Table 5.4; Fig. 5.4). Thin sections were described, ascribed soil microfabric types (MFTs) and microfacies types (MFTs), and counted according to established methods (Bullock *et al.* 1985; Courty *et al.* 1989; Courty 2001; Macphail and Cruise 2001; Stoops 2003; Goldberg and Macphail 2006). An overview of the soil micromorphological results for each thin section is presented here (Table 5.5), and the more detailed data is presented as an appendix (Appendix 7).

PHASE 1, 'TILTED BLOCK'

Analysis was carried out on samples from two monoliths, samples <40081> and <40082>, covering the transition through contexts 40056, 40057 and 40058. Context 40056 was interpreted as Thanet Sand, and the overlying, much darker (40057) was thought to possibly be a palaeo-landsurface (Fig. 5.1a).

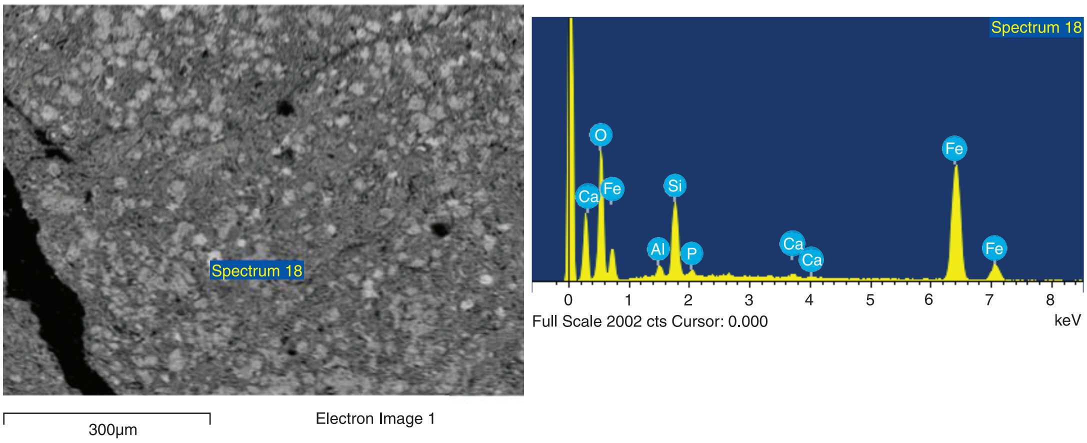

(a): Example of SEM/EDS (M40151B); Backscatter X-ray image and Spectrum of very fine iron nodules (e.g., 55.3% Fe, 1.07% P; see Table 5.4; Figs 5.3(a), 5.13(g)-(h)).

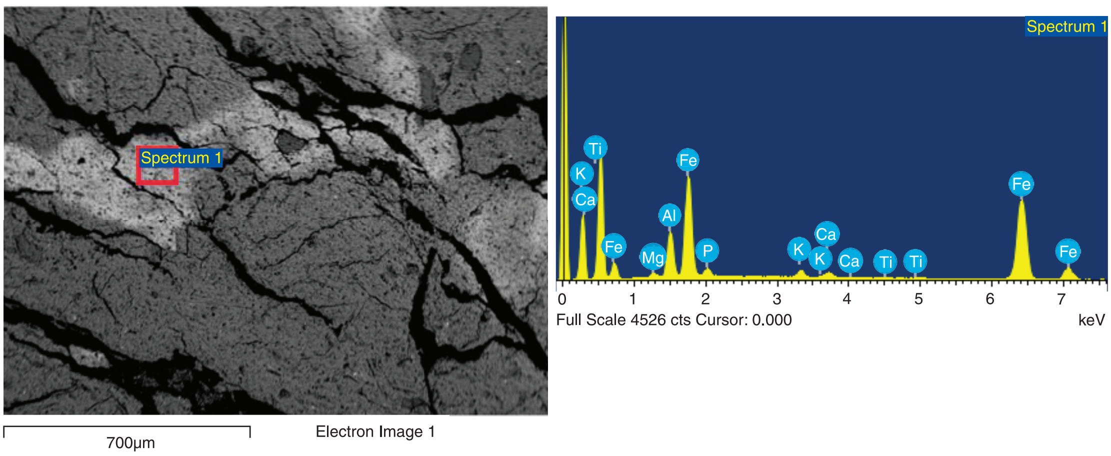

(b): Example of SEM/EDS (M40150A); Backscatter X-ray image and Spectrum of iron pan (e.g., 39.8% Fe, 1.35% P; see Table 5.4; Figs 5.3(b), 5.16(a)-(d)).

Figure 5.4 SEM/EDAX analyses: (a)–(b)

Table 5.5 Soil micro-morphology counts

Thin section	*Depth(cm)*	*Context - rev*	*Phase*	*Bulk sample no.* <>	*MFT*	*SMT*	*Voids*	*Gravel*	*Clay clasts (soil?)*	*Glauc.*	*Root traces*	*Organic traces*	*Ferrug. peat*	*Charcoal*
M40418A	4.5-12.5	40166/40158	7/6	-	E4	3a3, 3a1	10%		a* papules	f	a?			
M40418A	7-11(11-12.5)	40158	6	x40158	C1	5a1(3a3)	25%			*	aa(aaaa)	aaa	aaa frags	
M40418B	17-25	40158/40040	6/6a	-	E3	6a2/3a3	15%			*		aaaaa		aaa
M40418C	40-45	40040-40025	6a-5	-	E2	3a3	40%		?	*		a?	a?	
M40418C	45-48	40158-40040-40025	6-6a-5	-	E1	3a3, 3a4	35%		?	*		a	a	
M40149	35-43	40099, brownish	6	x40099	C3b	6a1	30%	(a-1)		*	a*	a		a*
M40150A	22-24(27)	40099	6	-	C3a	6a1	15%	(a-1)		*	aa	a		a*
M40150A	24(27)-38	40099/40103	6/6a	x40103-Fe pan	C2	5a1	25%	a-1	(aa)	*	aaa(aaaa)	aaa		a*
M40150B	22-38	40103	6a	x40103-Fe mottling	C1	5a1	25%			*	aa(aaaa)	aa		
M40151A	7-15	40103/40039	6a	-	B2	3a1(3a3)	30%			*	a*	a*		
M40151B	32-41	40039/40025	6a/5	x40039	B1	3a1, 3a2, 3a3	20-30%		(aa)	*	a*	aa	aaaa	a(aa)
M40365A	5-13	40078/40099	6	x40078	D3	3a1, 3a2, 3a3	25%	a-1		*	aaa	aaa	(a: org peat)	
M40365B	22-30	40099, brownish	6	x40099	B1	3a1, 3a3	25%			*	aaa	a		
M40365C	31-39	40099, brownish	6	-	B1	3a1, 3a2	10%			*	aaa	a		
M40323A	0-7	40039	6a	-	D2	4a2	10%			*	aa	aa?		
M40323B	7-13	40039	6a	-	D1	4a1	20%	*		*	(a)			a*
M40196	8.5-16.	40100	6	x40100-a; x40100-b	D2a	10a, 10b	10%	(a*)		*	a*			
M40195	13-21	40100 (sandy lenses)	6	-	D1a/D1b	9a1, 9a2	20%	f	(aaa)	f	a*?	a*		
M40194	32-40	40100 (stones/ artefact inclusions?)	6	-	C4a	7a1,7a2,7a3	10%	a-1		*		aa(?)		a*
M40193A	29-37	40100/40039	6/6a	x40039-top; x40039	C4b	8a1, 8a2	25%	a-1		*	a*	a*		
M40193B	37-45	40039	6a	-	C4b	8a1, 8a2	15%			*		?		
M40082	29-37	40057	1	x40057	A1	1a1, 1a2, 2a1	25%			fff	a	a		

Table 5.5 (continued)

Thin section	*Depth (cm)*	*Context - rev*	*Burned mineral??*	*Flint chip?*	*Clay pans*	*Intercal.*	*Void clay coats/infill*	*Secondary Fe*	*Fine impreg Fe oxide/pyr.*	*Secondary FeP*	*Thin burrows*	*Broad burrows*	*V. broad burrows*
M40418A	4.5-12.5	40166/40158						a					aa
M40418A	7-11(11-12.5)	40158				aa		aaaaa		aa?			
M40418B	17-25	40158/40040			aaaaa	aaa	aa				aaa		
M40418C	40-45	40040-40025					a	aaa			aaa		
M40418C	45-48	40158-40040-40025	a-1?				aa	aaaa					
M40149	35-43	40099, brownish		a-1?		aaaa		a					a
M40150A	22-24(27)	40099		a-1?		aa							
M40150A	24(27)-38	40099/40103				aa	a*	aaaaa	?		aa?		
M40150B	22-38	40103				aa		aaaaa		aa			
M40151A	7-15	40103/40039						aaaa			a*?	a*	
M40151B	32-41	40039/40025				aaa		aaaaa	aaaaa	a			
M40365A	5-13	40078/40099				aaaaa	aa	aa					
M40365B	22-30	40099, brownish			aaaaa			aaaa	(a:ex-pyr)				
M40365C	31-39	40099, brownish				aaa		aaa					
M40323A	0-7	40039			aa	aa		aaaa					
M40323B	7-13	40039	(a*)			aa		a					(aaaa)
M40196	8.5-16.5	40100	a	a-2	aa	aaaaa	aa	(aaaaa)					
M40195	13-21	40100 (sandy lenses)		(a*?)	aa	aaaa	aa	aaaa					
M40194	32-40	40100 (stones/ artefact inclusions?)	a*			aaaaa	aa	aaa	aaa				
M40193A	29-37	40100/40039				aaaaa	aa	aaa					
M40193B	37-45	40039	a-2	a-1?		aaaaa	aaa	aaaaa		?			
M40082	29-37	40057						aa				a	

* - very few 0-5%, f - few 5-15%, ff - frequent 15-30%, fff - common 30-50%, ffff - dominant 50-70%, fffff - very dominant >70%; a - rare <2% (a*1%; a-1, single occurrence), aa - occasional 2-5%, aaa - many 5-10%, aaaa - abundant 10-20%, aaaaa - very abundant >20%

Loss-on-ignition

The sequence through contexts 40058 and 40057 was highly minerogenic, increasing slightly down through the sequence, but with the lowest LOI values in the analysis (Table 5.3; Fig. 5.2a). This trend broadly continued into the underlying sediments, through the bottom part of (40057) and into (40056).

Soil micromorphology

M40082 (context 40057)

As Figure 5.5 shows, within context 40057 there is a boundary zone between firstly, non-calcareous moderately poorly sorted, coarse silty and fine and medium sandy and secondly, glauconitic medium sand-rich sediments with little fine material. The latter became, upwards, mixed with moderately sorted coarse silts and fine sands, sometimes with fewer glauconite, and mixed with clasts, and burrowed-in and washed-in weakly humic clay (LOI=1.22%). Glauconite is moderately weathered with some partially weathered grains (Loveland and Findlay, 1982); opaques include haematite. A relict thin (1.5-2mm) probable root channel is marked by iron hypocoatings. Iron staining also affects traces of organic matter.

This thin section records a moderately mixed junction between fine and medium non-calcareous glauconitic sands, and overlying silty glauconitic sands, and clayey silts, probably deposited as alluvium and recording diminishing energy. There has probably been some burrowing and rooting, the latter affected by secondary iron staining, which marks a minor amount of sediment ripening/soil formation here. Clayey deposits were probably weakly humic originally.

PHASE 6/6a, SOUTH OF TRENCH D (WEST SIDE OF SITE)

Analysis was carried out on samples from the sequence of four monoliths, samples <40196>, <40195>, <40194> and <40193>, down through the Phase 6 grey clay (40100) and into the underlying Phase 6a reddish-brown clay (40039) (Fig. 5.1b). Context 40100 included various variations in colour and texture, with some horizontal sandier horizons and some horizontal bands of faint reddish-brown staining. This area of the site was associated with the dense flint concentration south of Trench D.

Loss-on-ignition

The sequence down through contexts 40100 and 40039 was generally minerogenic, oscillating slightly through the sequence, but with a general downward trend from *c* 2.5% at the top of the sampled sequence, down to *c* 1% at the base of 40039 (Table 5.3; Fig. 5.2b). The slightly higher value (2.52%) of the brownish bulk sample from <40196> in (40100), as opposed to 1.9%

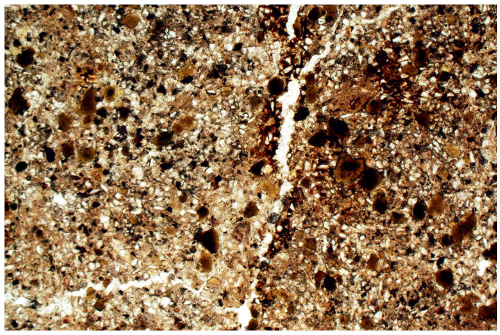

(a): Photomicrograph of M40082 (Context 40057); fine and medium glauconite fluvial sands. Note greenish to brownish weathered glauconite (Loveland and Findlay, 1982). Plane polarised light (PPL), frame width is ~4.62mm.

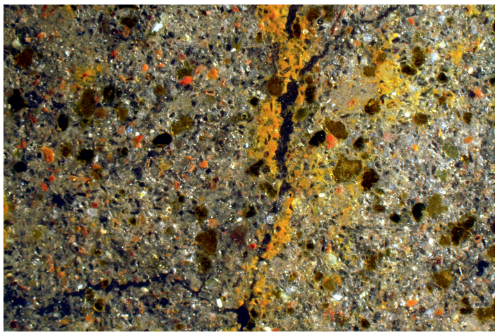

(b): As (a), under oblique incident light (OIL). A vegetated surface is recorded by iron staining relict of rooting. Glauconite is greenish. Opaque minerals seem to include red haematite.

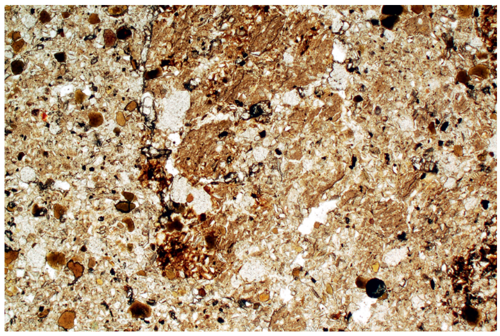

(c): As (a); upwards 40057 has iron-stained roots and burrows; the latter are affected by weak clay inwash (from overlying 40058?). PPL, frame width is ~4.62mm.

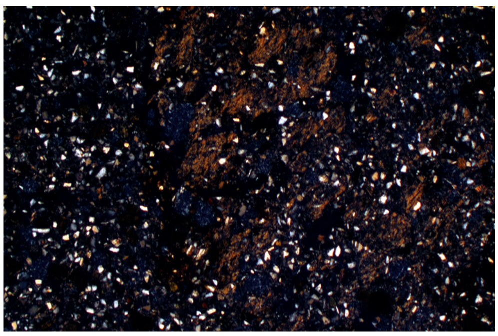

(d): As (c), under crossed polarised light (XPL). Note inwashed clayey burrow fills.

Figure 5.5 Thin Section M40082: (a)–(d)

from the adjacent greyish level, possibly suggests that the more reddish-brown layers within context 40100 in this part of the site may reflect a slightly higher remnant organic content. However, this proposed colour association evidently does not hold for the strongly reddish-brown underlying context (40039).

Soil micromorphology

M40193B (context 40039, lower)

This is similar to M40194 (see below) but more sandy, with three *c* 20-25mm thick layers of clayey fine sand (40% fine sand). There are textural clayey intercalations and iron staining throughout, but these are concentrated in the central layer where there are clay infills up to 3mm wide (Fig. 5.6) and an irregular boundary associated with clayey and sandy clay sediment mixing. Burrows are also iron stained in places. A 400µm-size patinated/calcined flint fragment and an 8mm-size angular flint flake (with possible traces of rubefication) were noted.

This sediment was originally a layered/laminated muddy fine sand (cf. M40151B, Fig. 5.3a), with sediment mixing, clayey intercalations and clayey infills with, for example, marked iron staining, all possibly indicative of trampling. This was possibly again related to large animals affecting an ephemeral surface (or surfaces), and/or by hominins, as the artefact inclusions may imply a hominin presence.

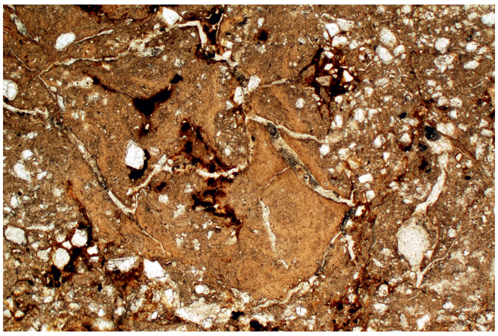

(a): Photomicrograph of M40193B (Context 40100); mixed clayey sands and clays, with clayey inwash feature. PPL, frame width is 4.62mm.

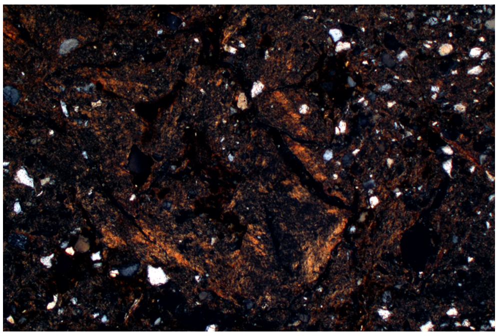

(b): As (a), under XPL; note orientated clay associated with this clayey infill.

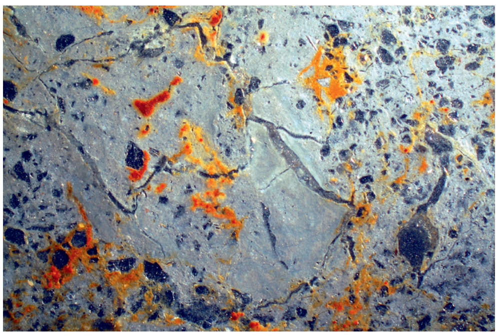

(c): As (a), under OIL. Sediment is essentially iron-depleted (gleyed/waterlogged conditions), but affected by later ferruginisation of probably organic staining.

Figure 5.6 Thin Section M40193B: (a)–(c)

M40193A (context 40100)

The sediment covered by this thin section is similar to that from below (M40193B), but contains more poorly sorted fine to coarse sands and sandy concentrations. There are very abundant textural intercalations, with associated closed vugh formation. Fewer ('many') and more weakly iron stained fabrics occur, however. There is an example of fine gravel and a root trace with ferruginised, once-organic very thin excrements present. It also seems to record muddy, possibly trampled, water-saturated sediments containing higher amounts of poorly sorted sands, compared to below; perhaps as the result of slightly increasing episodic fluvial activity.

M40194 (context 40100, stones/artefact inclusions?)

M40194 covers a heterogeneous, massive, compact iron-depleted clay and iron-stained clay (containing coarse silt and fine sand), with a sharp 2mm-size flint chip (Fig. 5.7 a; b). It is characterised by textural intercalations (associated with uni- and grano-striate b-fabric), which are sometimes silty clay in nature, and patches and infills of yellow-stained clay with fine (5-10µm) ferruginised amorphous organic material (very fine iron nodules/possible relict pyrite pseudomorphs?) (Fig. 5.7c; d). Trace amounts of very fine charcoal, blackened detrital organic matter and phytoliths are present, as well as examples of likely burnt mineral grains. There is fabric mixing of two major microfabric types.

It is a muddy and probably physically disturbed sediment, which was generally iron-depleted (gleyed) but which originally had organic sediment mixed in. The latter was originally affected by possible pyrite framboid formation (associated with decay of relict organic matter under hydromorphic conditions (Miedema *et al.* 1974; Wiltshire *et al.* 1994)) and oxidation/ferruginisation of this material and/or the fine organic material associated with it. Again, as in M40151B (40039) where phosphate concentrations occurred, wet sediment mixing in 40100 may have occurred alongside inputs of possible dung in an animal wallow (cf. Unit 4u at the Boxgrove freshwater pond, Macphail 1999). The occurrence of possible burnt mineral inclusions may indicate local contemporary fire, whether of hominin or natural origin is uncertain.

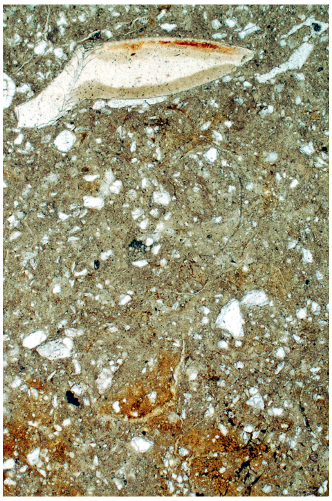

(a): Photomicrograph of M40194 (Context 40100), showing cracked flint flake and iron staining of generally iron-depleted sediment. PPL, frame height is ~4.62mm.

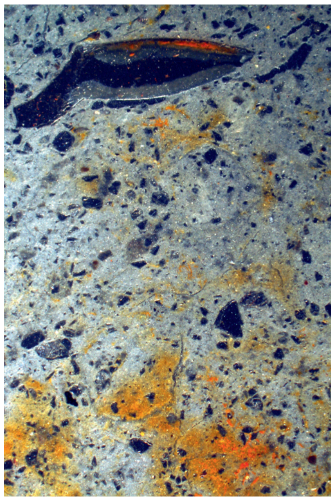

(b): As (a), under OIL. Note iron-staining on flint and generally iron-depleted waterlogged sediment.

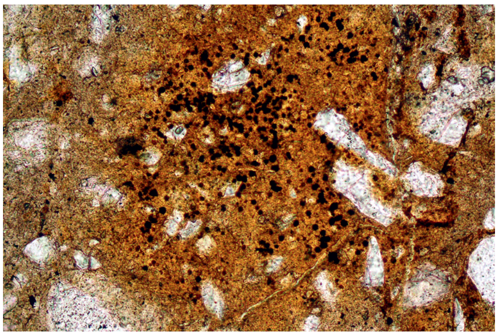

(c): Detail of (a), with very fine (5-10μm) iron nodules formed in iron-stained matrix. PPL, frame width is ~0.90mm.

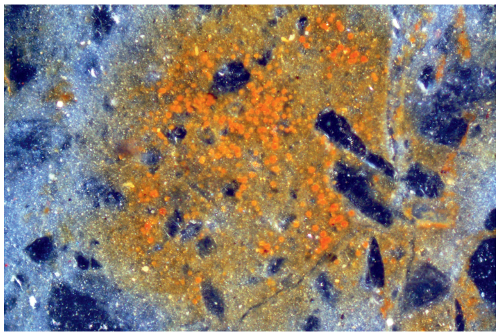

(d): As (c), under OIL. EDS on larger but perhaps similar nodules identified the presence of both Fe and P (see Figs 5.13(g)-(h)); these may also be possibly pseudomorphic of pyrite framboids.

Figure 5.7 Thin Section M40194: (a)–(d)

M40195 (context 40100, sandy lens boundaries)

This thin section is located along layered junctions between sandy microfacies (coarse silt, fine to very coarse sands with fine [max 5mm] flint gravel) and overlying a moderately, sandy clayey layer containing many fine gravel-size brownish clay clasts (as in M40196, see below) (Fig. 5.8). Upwards, is a greyish clayey layer where textural intercalations, matrix void coatings and clayey pans are abundant. There is weak to moderate iron staining throughout, possibly sometimes picking out relict amorphous organic matter. Both weathered and moderately fresh glauconite is present. Rare fine blackened/charred very fine organic matter occurs.

The thin section records a relatively high energy event/wash compared to the clayey deposits generally. First sands and fine gravels were deposited, followed by sandy clays containing gravel-size clay clasts (eroded 40100-type material from elsewhere, probably Tertiary deposits from high ground to the west; see Chapter 2), suggesting a lowering of energy and more muddy, possibly colluvial, deposition upwards. Lastly, muddy clayey sediments are deposited which are characterised by textural intercalations, matrix void coatings and clayey pans. Generally, this appears to be an upward-fining/decreasing energy sequence, the sand lens marking a localised relatively high energy deposition event, perhaps a fan/slopewash deposit.

M40196 (brownish over greyish)

This is a brownish clay loam, partially mixed with grey clay loam, and becoming more dominantly grey downwards (Fig. 5.3c). The microfabric is characterised by very abundant textural pedofeatures (intercalations, pans and matrix void coatings – and associated closed vughs) and iron staining. Fine channelling and fissuring affected the massive soil-sediment. Two flint chips (5mm and 10mm-in size, with a distinct outer patinated/stained zone), and an enigmatic embedded 'reddish' clay clast (*c* 1mm) occur (Fig. 5.9). Flints are also embedded in the soil-sediment matrix.

The sediment is a muddy mixed clay loam, with mainly iron-stained brownish sediment evident in the upper half of the slide and iron-depleted clay loam

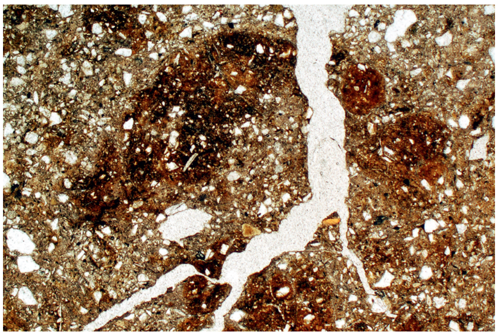

(a): Photomicrograph of M40195 (Context 40100); mixed sandy loam sediments contain rounded very coarse sand and gravel-size dark brown clay (as in M40195, Context 40100, above).PPL, frame width is ~4.62mm.

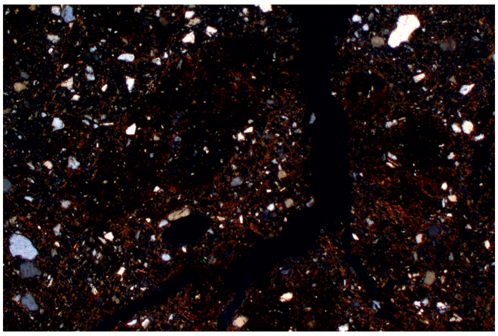

(b): As (a), under XPL; clay clasts act as embedded grains, indicating muddy slurry-like conditions of deposition, probably due to erosion and colluviation.

Figure 5.8 Thin Section M40195: (a)–(b)

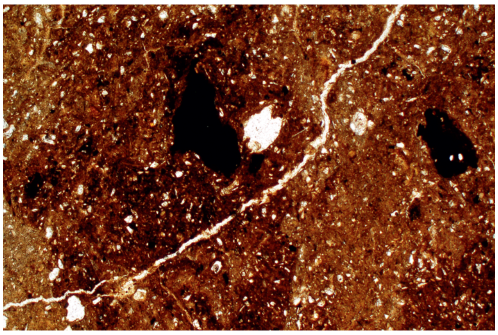

(a): Photomicrograph of M40196 (Context 40100) (see Fig 5.9(c)); highly heterogenous mixture of brown clay, iron depleted grey clay, and including opaque clay fragments. PPL, frame width is 4.62mm.

(b): As (a), under OIL. Note red (rubefied) colour of opaque clay clasts and other fine red mineral material. These could be fine fragments from a combustion feature.

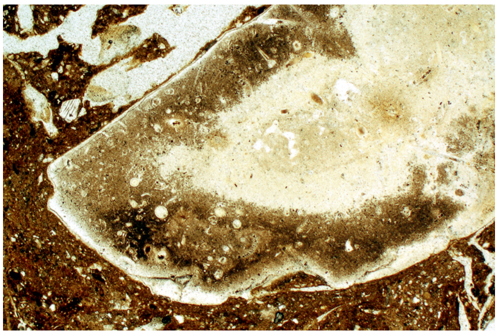

(c): As (a); fragment of 100mm-size fire-cracked flint. PPL, frame width is 4.62mm.

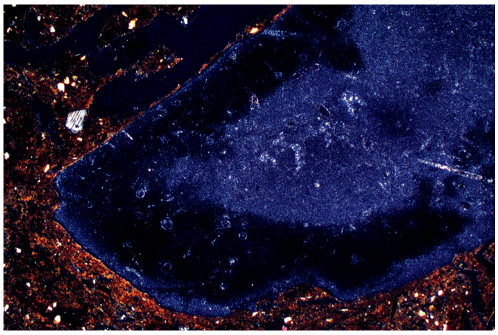

(d): As (c), under XPL. Flint occurs as an 'embedded grain' (aligned matrix clay around flint) within these once-muddy sediments.

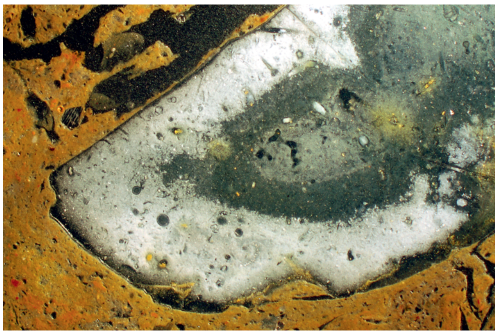

(e): As (c), under OIL, illustrating patination? rather than calcination (from burning) and cracked nature of the flint fragment.

Figure 5.9 Thin Section M40196: (a)–(e)

below. The upper part also shows mixed grey and brown microfabrics, and the inclusion of angular flint chips, and possible rubefied clay material, as two ~1mm-size fragments and as a scatter of very fine rubefied material. These materials may have been possibly a reworked relict of a combustion episode, but eroded from upslope and fragmented during downslope transport by colluvial processes. Thus, if this is evidence of contemporary burning, it would have been on higher ground to the west, rather than at the site, and, as above, it is uncertain whether it was of hominin or natural origin.

PHASE 6b/6a, TUFACEOUS CHANNEL (CENTRAL EAST SIDE OF SITE)

Loss-on-ignition analysis was carried out on samples from two short monoliths in the main longitudinal section through the tufaceous channel (Fig. 5.1c). The higher of these, monolith <40322>, covered the base of the mollusc-rich tufa (40070) and the top of the underlying grey clay (context 40103). The lower, monolith <40323>, covered the upper two-thirds of context 40039, the lowest bed of the Phase 6 clay, which was here stained strong faint yellowish-brown in patches, with occasional strong brown mottles. Two samples were taken from each of these monoliths, to form a sequence down through contexts 40070, 40103 and 40039 (Table 5.2). Thin sections were only analysed from two sub-samples from the lower monolith <40323>. The upper of the two thin section sub-samples, no. M40323A, was formed of the top 7cm of the monolith and covered the top part of context 40039, just below its junction with context 40103. The lower of the two thin section sub-samples was formed of the lower 6cm of the monolith, and covered roughly the middle part of 40039. It was also intended to examine thin sections from monolith <40322>, but this was unfortunately found to be unusable on delivery.

Loss-on-ignition

This sequence (Fig. 5.2c) reveals a close correlation between LOI and magnetic susceptibility χ, and a clear distinction between (40070), which has a higher LOI and χ, and the underlying contexts (40103 and 40039).

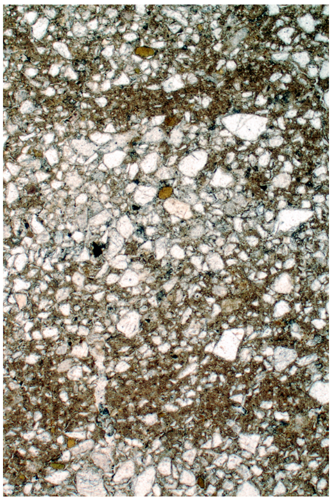

(a): Photomicrograph of M40323B (Context 40039 middle); relict clayey and sandy laminae. PPL, frame height is ~4.62mm.

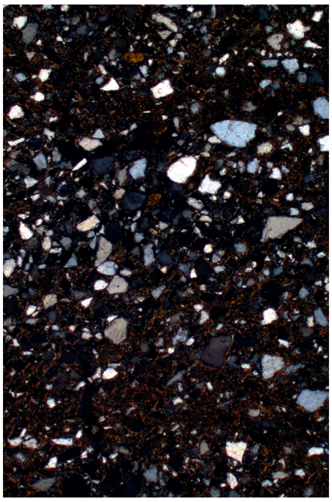

(b): As (a), under XPL. Note fine and medium subangular and angular quartz sand, and grano-striate b-fabric formed by muddy clay deposition.

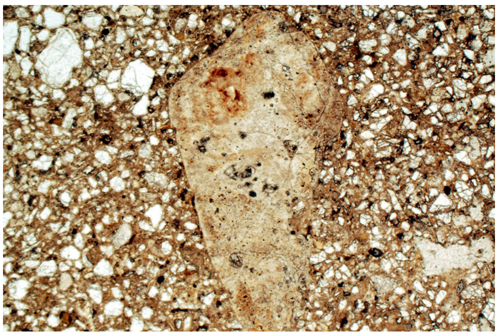

(c): As (a); gravel-size flint inclusion. PPL, frame width is ~4.62mm.

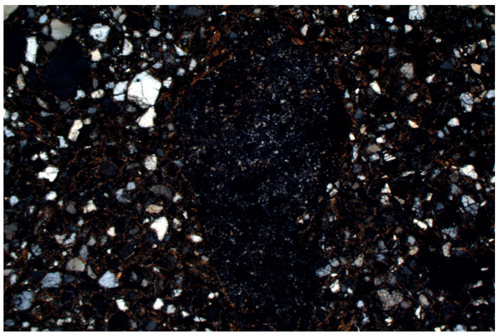

(d): As (c), under XPL; note birefringent clay around flint ('embedded grain'), suggesting inclusion in muddy sediment.

Figure 5.10 Thin Section M40323B: (a)–(d)

Soil micromorphology

M40323B (context 40039, middle)

As seen in this thin section, context 40039 is a massive, moderately well sorted clayey fine and medium sand. It also contains very rare fine gravel clasts, and relict sedimentary laminae (Fig. 5.10). Traces of very broad burrows and penecontemporaneous clayey inwash; intercalation and grano-striate formation were also noted. Clayey intercalations may reflect rooting and associated preferential channel formation. Rare iron staining (for example along the edge of very broad burrow?) and sedimentary laminae hypocoatings were found.

The thin section records moderately low energy muddy fine and medium sandy colluvial deposition, with penecontemporaneous very broad burrowing and clayey infilling. Minor secondary iron staining also affected the sediment.

M40323A (context 40039, upper)

Here, 40039 is a massive, moderately well sorted clayey fine and medium sand, with in the main a strongly iron-depleted fine fabric, which is generally very weakly humic, but appears, upwards, to have a series of thin (<1mm) once-humic (now-iron-replaced) pans. There are trace amounts of phytoliths present, probably derived from contemporary wetland vegetation. In the uppermost 5mm a scatter of 0.5mm-size clay clasts occur (Fig. 5.11). Iron also picks out many traces of probable fine rooting and voids around these clasts.

The sediment characteristics suggest moderately low, becoming lower, energy fine and medium sandy colluvial deposition, marked by thin rooting and periodic organic matter accumulation, possibly seasonal very thin peat formation. Lastly, inwash of eroded clay clasts is recorded. This all occurred under waterlogged conditions (hence iron depletion and organic matter panning), perhaps as the channel silted up. The sediment was affected by secondary but penecontemporaneous iron staining.

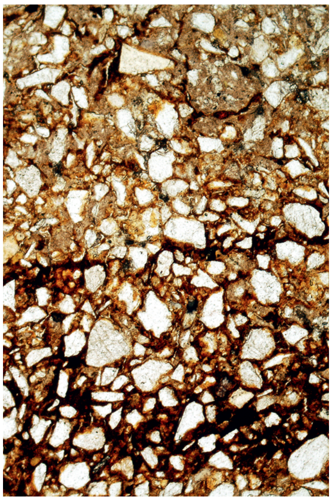

(a): Photomicrograph of M40323A (Context 40039 upper) showing 1mm-thick ironpans and overlying sands containing subrounded clasts of iron-depleted clay. PPL, frame height is ~4.62mm.

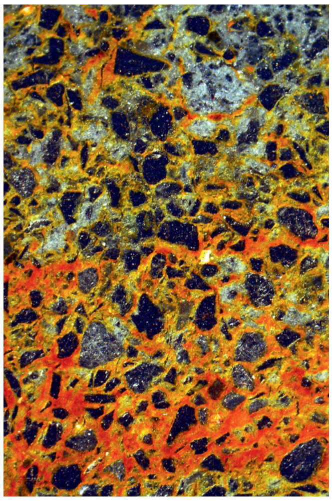

(b): As (a), under OIL. Note ferruginised ironpans. Iron appears to replace very thin once-humic laminae.

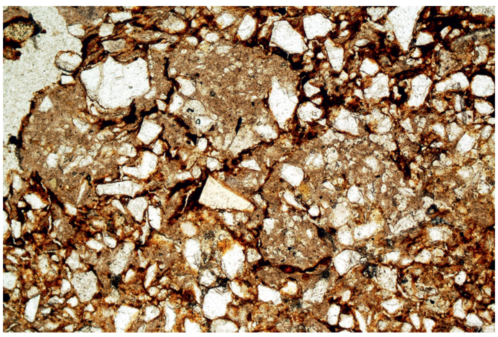

(c): As (a); detail of iron-depleted clay soil-sediment clasts, probably indicating colluvial deposition of eroded soil-sediments from upslope. PPL, frame width is ~2.38mm.

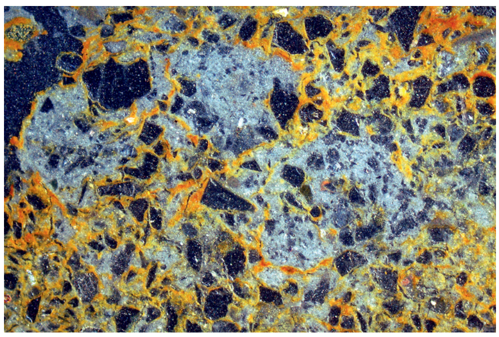

(d): As (c), under OIL. Soil-sediment clasts have become cemented by secondary iron deposition, possibly associated with relict fine rooting in places.

Figure 5.11 Thin Section M40323A: (a)–(d)

PHASE 6/6a, WEST END OF TRENCH C, NEAR ELEPHANT

Analysis was carried out on samples from one monolith, sample <40365>, covering the transition through contexts 40078, 40099 and 40103. This sample was taken at the west end of the south face of Trench C (Fig. 4.9), being the nearest vertical section to the elephant skeleton that could be obtained (Fig. 5.1d). By this stage, it was realised that organic-rich brown-stained horizons, such as contained the elephant (40078), were multiply present in this part of the site towards the base of the Phase 6 clays, and often faded away laterally, or merged with and separated from, each other. Nonetheless, the upper brown-stained horizon in sample <40365> was a lateral continuation of the same bed that contained the majority of the elephant bones and the associated flint artefacts. So this sample was not only subjected to sedimentological analyses, but also relatively intensive pollen analysis (Chapter 12).

Loss-on-ignition

The LOI values recorded in this sequence were quite low, with the values generally between *c* 2.00 and 2.50% (Fig. 5.2d; Table 5.3), although there was a minor peak towards the base of 40103 (at 405mm).

Soil micromorphology

M40365C (context 40103, with reddish-brown staining)

Recorded in this thin section is, generally, an iron depleted, very weakly humic clay, but with many ferruginised traces of roots, some possibly once-woody and up to 3mm in diameter. It is a waterlogged lacustrine clay, with sediments having acted as rooting medium for wetland, and possibly woodland, plants.

M40365B (context 40099, with reddish-brown staining)

This is a mainly iron-depleted clay, characterised by *c* 1mm-thick clay panning (sedimentation), with silt-rich clay loam infilling along possible relict root channel-fills; the latter are marked by iron staining and relict likely hypocoatings. Relict root features are 3-5mm wide; some show ferruginised traces/oxidised traces of probable pyrite framboids associated with roots (Fig. 5.12). These are waterlogged clay sediments deposited as muddy pans, perhaps associated with very low energy alluvial events/flooding. Sediments were rooted by plants, possibly shrubs/woodland, and more silty clay loam infilled these on decay.

M40365A (context 40099-40078 transition)

This is a weakly humic clayey sediment with fine organic fragments and (possibly monocotyledonous) root traces and common patches of partially bedded silty clay loam (40078) over iron-depleted clayey (40099). Context 40078 includes blackened relict plant/root fragments, up to 1mm in size (red and black under PPL); overall organic matter content is reflected in 2.44% LOI. Textural intercalations and associated matrix coatings, and fabric mixing associated with relict channels and fissures.

Layered, weakly humic remains of a putative junction between monocotyledonous minerogenic peat and minerogenic sediments are present, with evidence for flood wash bringing in silts; hence mixing down profile along old root channels. Rooting down through waterlogged clayey sediment caused fabric disruption, mixing and intercalations, typical of shallow lakes that dry out (Cruise *et al.* 2009). This sediment records a period of moderate stasis, possibly with flooding of inwash silts and peat growth.

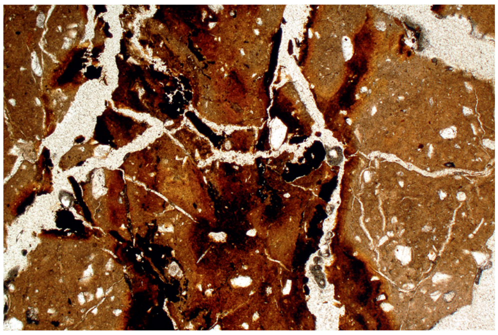

(a): Photomicrograph of M40365B (Context 40098); root traces in waterlogged clayey sediment. PPL frame width is ~4.62mm.

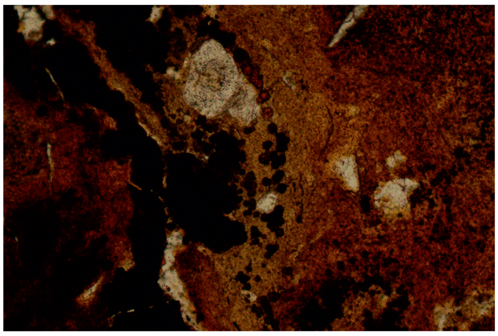

(b): Detail of (a), showing ferruginised pyrite (framboid) pseudomorphs associated with root decay. PPL, frame width is ~0.90mm.

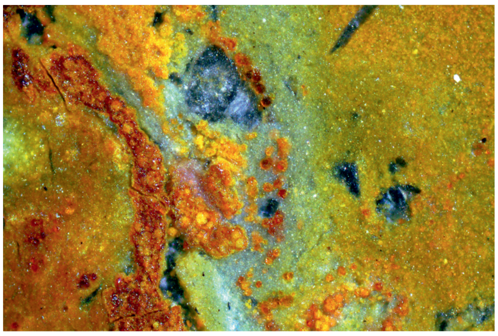

(c): As (b), under OIL.

Figure 5.12 Thin Section M40365B: (a)–(c)

PHASE 6/6a/5, CENTRAL WEST SIDE OF SITE, NEAR ELEPHANT

Analysis was carried out on samples from the sequence of five monoliths down through the Phase 6 clay in the central part of the main west-facing section (Fig. 4.5), and into the underlying Phase 5 clay-laminated sands: monoliths <40148>, <40149>, <40150>, <40151> and <40152> (Fig. 5.1e). This monolith sequence was likewise located reasonably close to the elephant, and preserved the full range of contexts through the lower Phase 6 stratigraphic sequence (apart from Phase 6b, the tufaceous channel, which was not present in this part of the site).

Loss-on-ignition

In this sequence, there is a clear peak in LOI and magnetic susceptibility χ at 102.5–111cm (corresponding with the top and upper part of context 40103 (Fig. 5.2e; Table 5.3). It should also be borne in mind that organic matter in the various contexts will have been subject to post-depositional decomposition; the LOI recorded therefore underestimates the original organic matter content, so this peak is likely to be associated with soil development and surface exposure. Sediments become increasingly minerogenic towards base of sequence (contexts 40039 and, especially, 40025).

There was, however, no peak in LOI or magnetic susceptibility associated with the brown-stained and apparently humic-rich context 40078, although the values were marginally higher than for the grey clay above and below.

Soil micromorphology

M40151B (context 40025/40039 transition)

This thin section includes a partially layered, partially coarsely mixed non-calcareous sediment composed of clays, silty clay, fine and medium sands and ferruginised once-organic sediment (Fig. 5.3a). Silty clays are composed of mixed silt and clay fine laminae. Charcoal as both rare fine (max 800µm-size monocotyledonous charcoal) and occasional very fine material occurs alongside very fine blackened (detrital) organic material, and phytoliths are present (Fig. 5.13a; b).

Patches of totally ferruginised organic matter including plant fragment pseudomorphs occur (current LOI is 1.88%) (Fig. 5.13c; d). Sediments are also characterised by textural intercalations and associated matrix embedded grains and matrix void coatings, some stained yellow. Sediments have evidence of mottling: iron-depleted and iron-stained areas. Rare fine sand-size yellow isotropic nodules/infills, and fine ferruginous nodules are iron phosphate formations, as confirmed by SEM/EDS (Table 5.4; Fig. 5.13e; f). Generally iron-depleted sediments (2.41-3.90% Fe); patches of iron staining also includes phosphate (22.5-43.7% Fe, 0.55-0.76% P, *n*=3). In iron-stained sediments strongly developed very fine (*c* 30µm) iron nodules are more phosphate-rich (38.7-67.1% Fe, 0.97-1.33% P, *n*=4; Fig. 5.13g; h). The sediment overall is characterised by slight phosphate enrichment, 0.556 mg g^{-1} phosphate-P (Table 5.3).

This deposit was originally a bedded and laminated sediment composed of weakly humic clays, silts, and occasionally medium sands, with patches (possibly inclusions) of peaty material, which are now ferruginised and include plant pseudomorphs. The presence of these organic traces, and charcoal including likely monocotyledonous material, suggests the local presence of wetland (marsh) and, possibly, local incidences of burnt vegetation, and later possible rooting by woody plants: possibly a hydroseral plant succession. Contemporary fabric mixing and associated intercalations, matrix coatings, and yellow phosphate staining and very fine nodule formations that are enriched in P, alongside overall slight phosphate enrichment may infer animal trampling and defecation, possibly in a wallow. Such phosphate enrichment was attributed to large animal concentrations at the Q1B waterhole site at Boxgrove (Macphail *et al.* 2001).

M40151A (context 40039, upper)

Upwards, 40039 continues as massive non-calcareous clay sediments (few sand inclusions), with marked iron-staining overlying 40103. This occurs partially as strongly iron-depleted clay in uppermost 20mm of the thin section. There are infill features (30mm deep by 4.5mm wide curved 'fill'), burrows, once humic peds and excrements, demarcated by strong iron-staining. Sands are only present in rare broad burrow fills. Clays are seemingly less humic compared to lower down, and only very fine charred/blackened detrital organic matter noted.

Minerogenic and sometimes peaty context 40039 develops upwards into a ripened minerogenic wetland clayey sediment which appears to have developed as a topsoil, possibly a hydroseral succession. Here, there are burrows, peds, roots and excrements of relatively humic soil showing marked iron impregnation (Fig. 5.14). Overlying iron-depleted context 40103 is probably a flood clay, recording inundation of the site. The transformation of the buried topsoil through ferruginisation is common to other examples of flood inundated soils, for example Upper Palaeolithic and Early Mesolithic Three Ways Wharf, Uxbridge; Boxgrove Unit 5c and newly inundated coastal analogue sites (Lewis *et al.* 1992; Macphail 1999 and 2009; Lewis and Rackham 2010; Macphail *et al.* 2010).

M40150B (context 40103)

The sediment in this thin section is a massive clay containing small amounts of coarse silt, fine and medium sand. The clay has fissures and relict channels, some with probably ferruginised (woody) root pseudomorphs (0.5-2.5mm; with traces of very thin ferruginised excrements) (Fig. 5.15). The sediment is mottled with iron depleted and iron stained areas and other

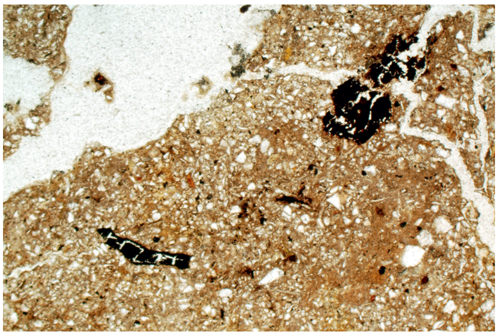

(a): Photomicrograph of M40151B (Context 40039) (see Fig 5.3(a)); mixed weakly humic clays and coarse silts, with very fine and fine charcoal. PPL, frame is ~4.62mm.

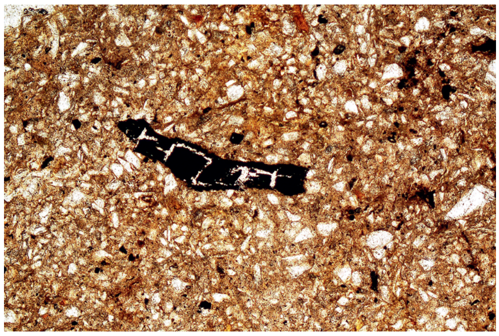

(b): Detail of (a), showing possibly inclusion of monocotyledonous charcoal. PPL, frame width is ~2.38mm.

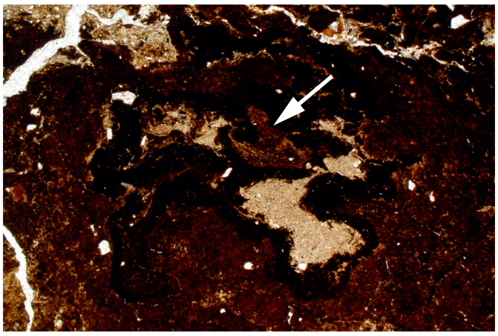

(c): As (a); iron stained area, relict of peat(?). Note possible ferruginised woody(?) root and plant cells (arrow). PPL, frame width is ~4.62mm.

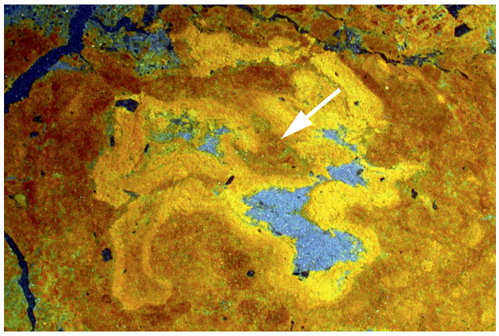

(d): As (c), under OIL.

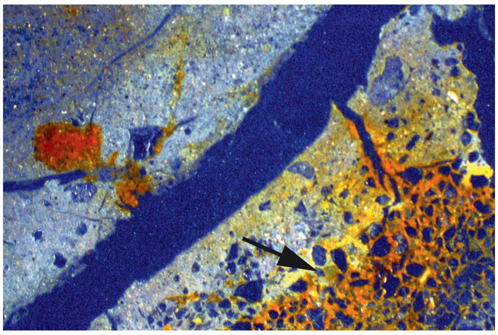

(e): As (a); iron-depleted and iron-stained layers. Some iron staining is yellowish and infills voids (arrows). OIL, frame width is ~4.62mm.

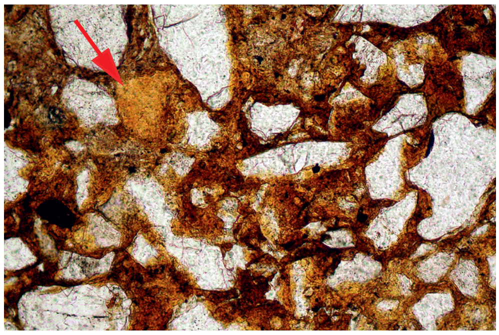

(f): As (e), detail of amorphous Fe-P void infill (arrow) and grain coatings. PPL, frame width is ~0.90mm.

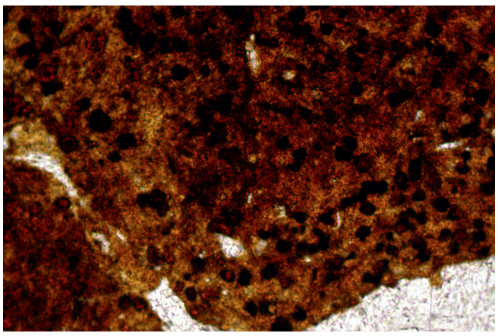

(g): As (a); very fine (~30µm), strongly-formed iron nodules (38.7-67.1% Fe) in iron-stained area; nodules also include 0.97-1.33% P (Table 4, Fig 5.4(a)). PPL, frame width is ~0.90mm.

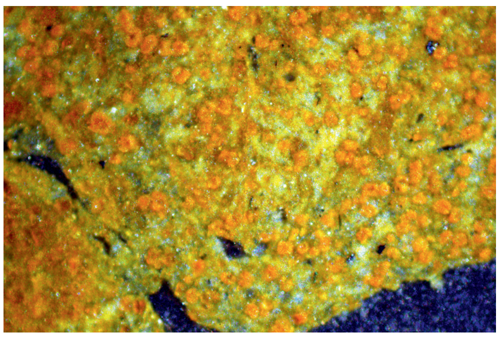

(h): As (g);Fe-P nodules under OIL.

Figure 5.13 Thin Section M40151B: (a)–(h) possible root stains. Some channels have iron-depleted hypocoatings. There is an example of a channel with a leached/iron-depleted clay fill. These appear to be 'basal' lacustrine clay sediments, containing scattered small amounts of coarse silt, fine and medium sand, possibly locally blown-in/washed-in. This clay acted as a rooting substrate, possibly for woodland, as is suggested by the presence of woody roots (some being dominated by small invertebrate mesofauna). The sediment was also affected by shrinking and swelling (possibly an

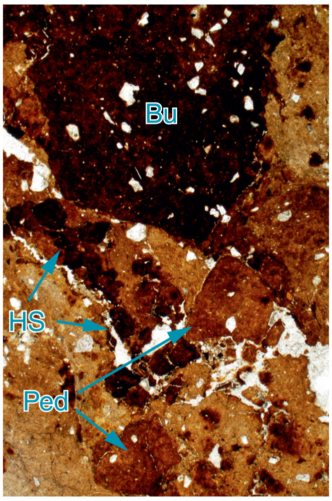

(a): Photomicrograph of M40151A (uppermost 40039); iron-stained remains of flooded soil, with ferruginised once-humic very broad (earthworm?) burrow (Bu), humic soil excrements (HS) and bio-mixed peds (Peds). PPL, frame height is ~4.62mm.

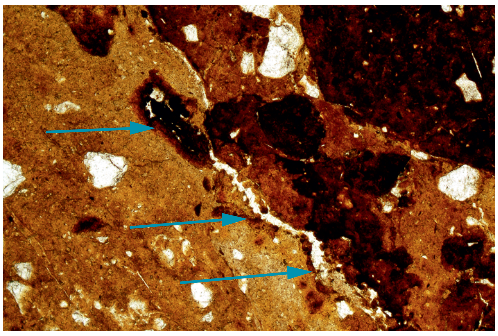

(b): Detail of (a); humic soil excrements associated with ferruginised root trace (arrows). PPL, frame width is ~2.38mm.

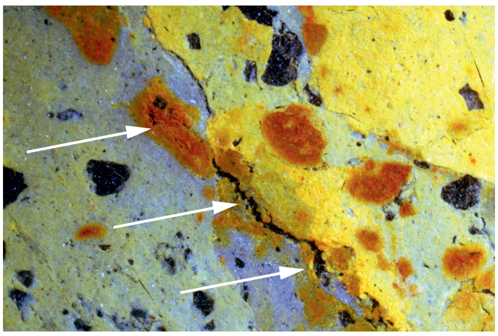

(c): As (b), under OIL.

Figure 5.14 Thin Section M40151A: (a)–(c)

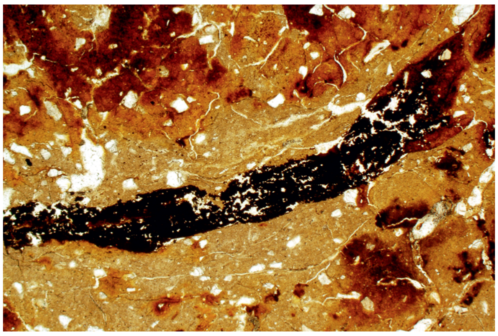

(a): Photomicrograph of M40150B (Context 40103); iron-mottled relict soil, with strongly ferruginised root. PPL, frame width is ~4.62mm.

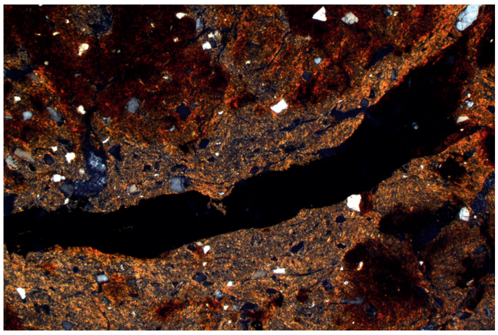

(b): As (a), under XPL; note clayey textural pedofeatures from inwash around this root and infilling the root channel.

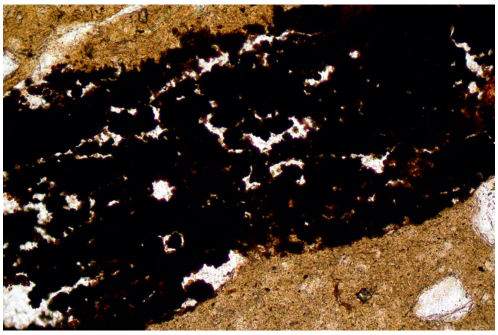

(c): As (a), detail of ferruginised root remains and likely very thin and once-organic excrements of mesofauna. PPL, frame width is ~0.90mm.

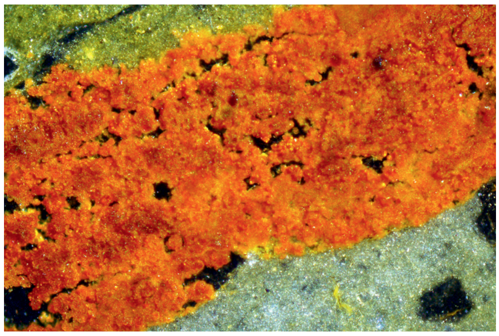

(d): As (c), under OIL.

Figure 5.15 Thin Section M40150B: (a)–(d) effect of woodland growth/evapotranspiration), marked iron depletion (and possibly clay break-down at times) and iron staining, all hydromorphic/gleying effects (Bouma *et al.* 1990). Enigmatic high measurements of LOI possibly relate to woody root traces, while enhanced P is probably secondary and linked to iron-staining (Thirly *et al.* 2006). This context could represent a woodland subsoil gley horizon (Bg/Cg horizon).

M40150A (context 40103/40099 transition)

Context 40103

This is similar to context 40103 in M40150B, below (see Fig. 5.1e), but with a (sloping?) concentration of iron staining along the uppermost 10mm of this context, forming an iron pan (Fig. 5.16a-d). This is partially made up of a concentration once-humic burrows and channel (fills), and in places 1mm-size 'soil' clasts

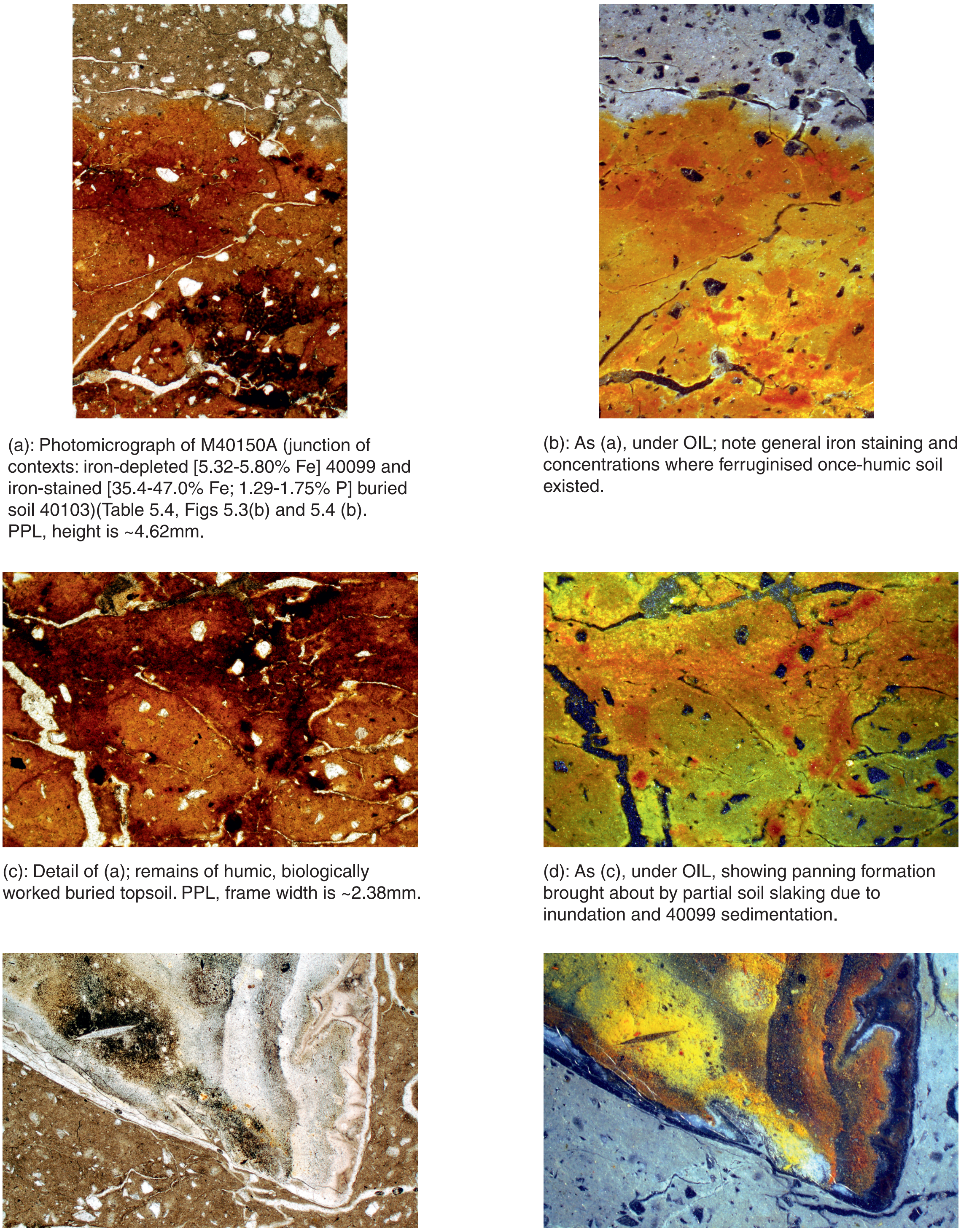

(a): Photomicrograph of M40150A (junction of contexts: iron-depleted [5.32-5.80% Fe] 40099 and iron-stained [35.4-47.0% Fe; 1.29-1.75% P] buried soil 40103)(Table 5.4, Figs 5.3(b) and 5.4 (b). PPL, height is ~4.62mm.

(b): As (a), under OIL; note general iron staining and concentrations where ferruginised once-humic soil existed.

(c): Detail of (a); remains of humic, biologically worked buried topsoil. PPL, frame width is ~2.38mm.

(d): As (c), under OIL, showing panning formation brought about by partial soil slaking due to inundation and 40099 sedimentation.

(e): As (a), edge of 12mm-size angular flint flake (see Fig 5.3(b)). PPL, frame width is ~4.62mm.

(f): As (e), under OIL; note iron-stained flint and iron-depleted sediment matrix.

Figure 5.16 Thin Section M40150A: (a)–(f) cemented by infills of sometimes strongly ferruginised (once-humic) fine soil (cf. <40151>). Trace amounts of very fine charcoal and a 6mm clast of rounded flint gravel were noted. A marked high LOI (3.63%) and enriched phosphate-content (1.77mg g^{-1} phosphate-P) were found in the initial bulk analysis (Table 5.3). SEM/EDS studies measured 35.4-47.0% Fe and 1.25-1.75% P in the iron-pan.

The uppermost part of 40103 appears to be a possible ripened sediment/soil surface, showing: firstly, slight truncation in places; secondly, traces of rooting and small mesofauna burrowing; thirdly, very locally eroded and transported ripened soil/sediment clasts; and fourthly, local inwash of humic fine soil. This may be a possible buried ripened soil that may have had short-lived woodland cover, before being affected by inundation and renewed sedimentation (context 40099). Gentle inundation caused slaking and structural collapse/formation of intercalations and void matrans, and erosion of local soil/sediments, and inwash (see references employed for M40151, cf. Holocene inundation sites along the Thames (Macphail and Crowther 2009)). This buried 'topsoil' interpretation is consistent with LOI and enriched phosphate probably also reflects this and 'geogenic' concentration of P due to groundwater movement (Thirly *et al*. 2006).

Context 40099

The lowermost part of this context is an iron depleted, very weakly humic clay containing rare detrital fine organic material, blackened (organic, possibly monocotyledonous) root traces and traces of charcoal. It includes a sharp flint chip (12mm) (Fig. 5.3b; Fig. 5.16a;b; Fig. 5.16e; f). Occasional intercalations and matrix infills, and strongly leached fissure and channel hypocoatings were noted. Bulk analyses record 2.26% LOI, 0.194 mg g^{-1} phosphate-P (Table 5.3). Iron-depletion was confirmed by SEM/EDS (Table 5.4).

These massive iron-depleted, possibly lacustrine clay sediments, show rooting (by wetland plants: blackened organic monocotyledonous root traces), and inclusions of detrital organic material including trace amounts of very fine charcoal. An anomalous 12mm size flint chip is very likely of anthropogenic origin, and, more specifically, is almost certainly part of the knapping activity associated with the nearby elephant skeleton. We are here at the north-west edge of the recovered lithic concentration around the elephant (see Chapter 17), and also at the same stratigraphic horizon. Strong leaching has affected the sediment, hence moderate organic matter preservation and markedly low phosphate content.

M40149 (context 40099/40078 transition)

This is an iron depleted clay, as below, with abundant sedimentary clayey intercalations, including a 4mm-thick layer/fill at 410mm depth. A 2mm flint chip is present, as an 'embedded grain' (Fig. 5.17a; b). Near the top, trace amounts of amorphous organic matter inclusions occur in channels. Very weak trace amounts of iron hypocoatings occur.

This thin section records continued muddy lacustrine/wetland sediment accumulation, with another flint chip from the knapping activity around the elephant. Inclusions of preserved amorphous organic matter (40078) may stem from inwash from adjacent areas.

PHASE 7/6/6a, NORTH SIDE OF TRENCH B, CENTRAL PART OF SITE

Analysis was carried out on samples from two monoliths, samples <40418> and <40419>, covering the transition from the base of Phase 7 (context 40166) through to the top of Phase 5 (context 40025), where Phase 6 was reduced in thickness to a particularly black, humic-looking upper bed (context 40158) and a pale grey interdigitating sandy/clayey lower bed (context 40040) (Fig. 5.1f).

Loss-on-ignition

The LOI data show a series of peaks corresponding with the dark context 40158, with a particularly high value of 6.68% in its upper part (Fig. 5.2f; Table 5.3). This very high peak is almost certainly associated with soil (and possibly peat) formation, and the secondary peaks at 44.5 and 56-66cm also seem likely to be associated with periods of soil development and/or surface exposure. As

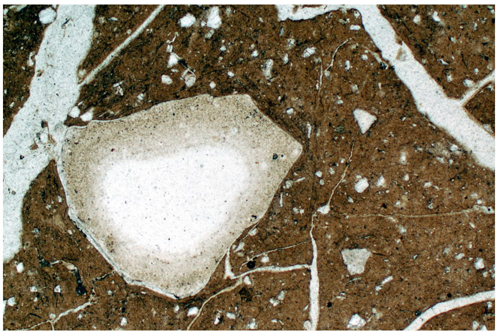

(a): Photomicrograph of M40149 (Context 40099/40078), containing angular flint fragment. PPL, frame width is ~4.62mm.

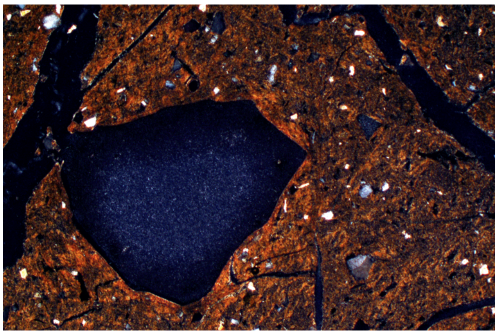

(b): As (a), under XPL. Note oriented clay around this flint fragment (embedded grain), caused by its deposition into a muddy water-saturated clay.

Figure 5.17 Thin Section M40149: (a)–(b) mentioned above, organic matter will have been subject to post-depositional decomposition, so this context would originally have been significantly enriched in organic content.

Soil micromorphology

M40418C (contexts 40040-40025/40158)

Contexts 40040-40025/40158
As seen here, these contexts are composed of laminated moderately well sorted coarse silts and very fine sands, with patchy 'layer'/infills of clay with occasional ferruginised very fine organic matter and phytoliths present (Fig. 5.18a,b). Very thin iron pans associated with sandy laminae appear to be associated with relict amorphous organic matter and involved with pseudomorphs of very thin relict excrement.

These appear to be fluvial coarse silts and very fine sands, perhaps resulting from seasonal (spring) alluviation, with winter periods of low energy clay deposition, forming infills. Sand laminae also sometimes associated with thin peat formation and its partial working by small invertebrates, again suggestive of seasonality. It may represent relatively cool climate, near-channel alluviation.

Lower context 40158
This is moderately well sorted, massive sediment, which is sometimes laminated with very fine to fine sands that also includes coarse silt and medium sand. Many thin burrows, examples of clayey inwash down fine (1mm) channels (possibly decayed rootlets) and very thin stringers (possibly of ferruginised organic matter) inwash were also recorded. These channel mainly fine sands, were burrowed and rooted, and thus were probably episodically/seasonally exposed. Possibly humic matter from above (see M40418A and M40418B) filtered down and became ferruginised. Clayey sediments above were introduced down-profile along empty relict root channels.

M40418B (context 40158/40040)

This thin section is mainly composed of laminated very humic clayey fine sands and humic clays, with abundant included fine amorphous organic matter and fine charcoal (100-250μm), and few fragments of amorphous peat; it is increasingly humic upwards. An example of a horizontally oriented 5mm long very thin blackened monocotyledonous leaf/leaves fragment occurs (Fig. 5.19a-d). Humic clays sometimes occur as clayey pans and infills. Minor thin burrowing has occurred. The context has markedly high LOI as discussed above (Fig. 5.2f; Table 5.3).

These are laminated peaty clays and peaty sands, horizontally deposited under low to moderately low energy conditions, allowing horizontal deposition of detrital leaves, fragments of pure peat and ubiquitous fine and very fine charcoal. Organic matter shows no sign of being ferruginised. These are perhaps low energy (seasonal?) minerogenic peats associated with a burned landscape – wildfires and /or fire-managed.

M40418A (contexts 40158/40166)

Upwards, context 40158 sediments become less humic and contain less fine detrital organic material, being clayey deposits, but here also have developed marked (many) iron-staining of organic traces.

These are laminated peaty clays and peaty sands, horizontally deposited in low to moderately low energy conditions, allowing horizontal deposition of detrital leaves, fragments of pure peat and ubiquitous fine and very fine charcoal. The humic content seems rather less, and shows much ferruginisation compared to this context below in M40418B. Again, these may be the result of low energy (seasonal?) minerogenic peat formation associated with burned landscape, most likely wildfires, but here have been affected by penecontempo-

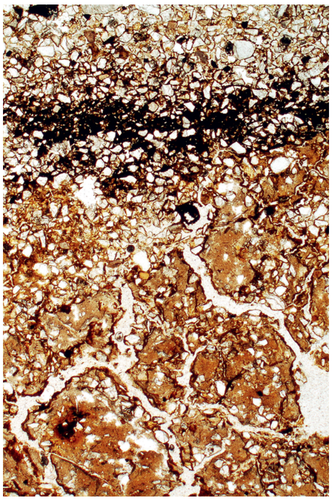

(a): Photomicrograph of M40418C, Context 40025/40040 transition. Sands with clayey infills sealed by ironpan that is relict of a thin peat layer. PPL, frame height is ~4.62mm.

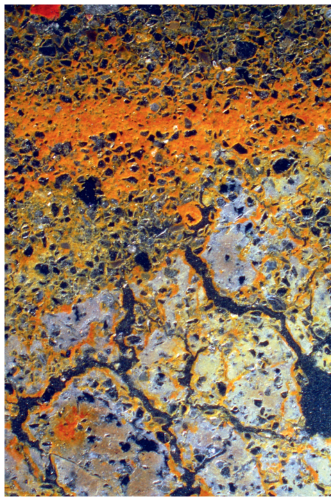

(b): As (a), under OIL; note iron-depleted clay and later ferruginisation, and ironpan formation.

Figure 5.18 Thin Section M40418C: (a)–(b)

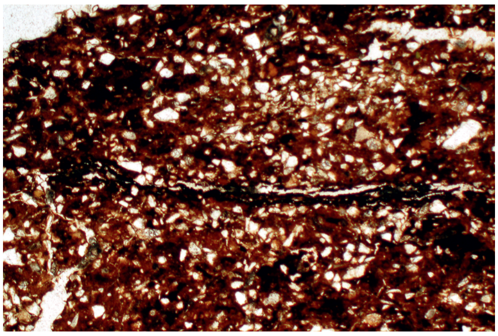

(a): Photomicrograph of M40418B, Context 40158, clayey and peaty fine sands, with 6mm-long horizontally oriented blackened monocotyledonous leaf(?). PPL, frame width is ~4.62mm.

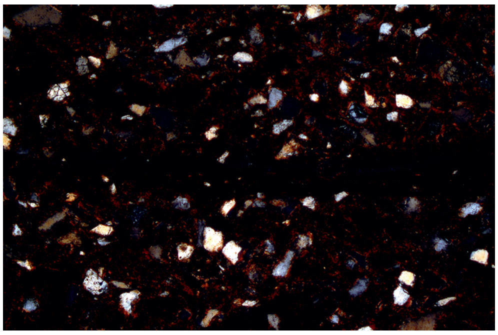

(b): Detail of (a), under XPL, showing grano-striate birefringence of (muddy) clay. Frame width is ~2.38mm.

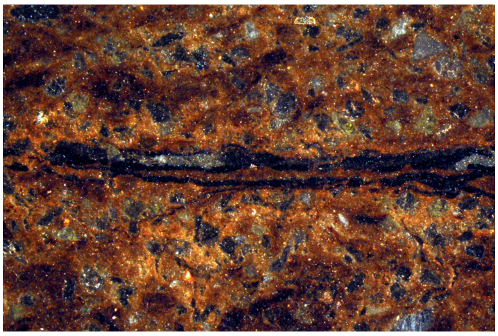

(c): As (b), under OIL.

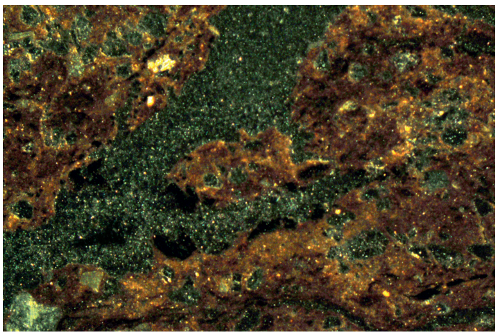

(d): As (a); example of charcoal (fragmented on sediment drying); OIL, frame width is ~2.38mm.

Figure 5.19 Thin Section M40418B: (a)–(d)

raneous iron movement and staining affecting this upper part of the context.

Context 40166

In contrast to 40158, context 40166 is highly minerogenic. It is composed of massive and finely laminated, poorly sorted sands with coarsely mixed clay fragments (clay papules), and only shows a trace amount of iron staining, and occasional broad burrows.

Minerogenic poorly sorted laminated sediments record a cessation of 'peat' formation here and probably locally, and show instead slight variations in energy and erosion of sands and more clayey sediments. Possible iron depletion here led to ferruginisation of organic fraction of sediments below.

DISCUSSION

Post-depositional processes

The chief post-depositional processes of interest at this site are: a) iron depletion, b) oxidation of organic matter (often alongside its ferruginisation), c) iron migration and d) phosphate migration. Other processes, such as compaction, possible decalcification etc., which often occur in Pleistocene soil-sediments (cf. Boxgrove), are not specifically relevant to interpretations of the micromorphology here.

a. Iron-depletion is a very important phenomenon at Southfleet Road and is probably the chief process resulting in 'grey' layers. Such gleyed layers occur through hydromorphism where water saturation (and associated extant water tables) led to iron reduction (Fe^{3+} to Fe^{2+}), and the loss of mobile reduced iron (Duchaufour 1982; Bouma *et al.* 1990). This process was probably penecontemporaneous with MIS 11 site formation, and continued sedimentation; the soil associated with the palaeo-landsurface at the top of the Lower Loam at Barnfield Pit itself records hydromorphic effects on soils buried by ensuing alluvial sedimentation and the associated rise in water table (Kemp 1985). Some of the effects of mobile iron at the Southfleet Road site are noted below.

b. Likely oxidation of organic matter and plant remains at the site is noted from the chemistry (see above; Crowther, Appendix 2), and even the most humic context (40158 in thin section M40418B), only recorded a 6.68% LOI. It can be noted that ferruginisation appears to have affected *some* probably once-humic contexts, for example context 40103 (M40150A) which records LOI of 3.63% (40158, in M40418B), seems anomalously unaffected by ferruginisation. In addition, roots for instance show poor pseudomorphic replacement in sometimes otherwise iron-depleted sediments. In relation to this, ferruginised root traces show relict remains of probable pyrite spheroids, where pyrite had formed in association with organic materials under original waterlogged conditions (eg root decay) (Miedema *et al.* 1974; Wiltshire *et al.* 1994), and then become transformed to amorphous iron oxide. It is possible that concentrations of amorphous organic matter may also have been ferruginised (see below). As a comparison, the iron pan at Boxgrove most commonly occurs as a strongly oxidised once-humic minerogenic peat (0.80-0.90% organic C), and only under exceptional conditions of burial has it retained some of its original organic character (5.30% LOI at BH5: Macphail *et al.* 2010). Context 40158 (M40418B) thus must also have experienced a similarly unusual burial history; perhaps it remained water saturated until deep burial sealed it. This is suggested because ferruginisation of relict plant material and other organic remains can be a penecontemporaneous process, as observed at the analogue site of Wallasea Island, Essex (Macphail *et al.* 2010) and in hydromorphic soils in general (Bouma *et al.* 1990).

c. Iron migration, as noted above, is related to hydromorphic iron-depletion (gleying), and led to the reprecipitation of iron as 'ironpans' and iron mottled zones often seemingly associated with once-organic sediments. In addition, ironpans can develop along hydrological boundaries. It is likely that iron-panning (max 47.0% Fe) occurs at context 40103 (<40150A>) below iron-depleted (max 5.80% Fe) context 40099, because (1) 40103 appears to be a relict 'topsoil' (3.63% LOI) and (2) there appears to be a hydraulic barrier between this soil and inundation sediment 40099 (see below).

d. Phosphate migration and deposition, is often associated with (c), and possibly sometimes with (b). In the first instance, mobilised phosphate within the soil-sediment groundwater system has apparently migrated from its original location/source and been reprecipitated along with iron in ironpans and iron mottles (max 1.75% P). This migration of phosphate has been noted previously in waterlogged sediments (Cruise *et al.* 2009; Thirly *et al.* 2006). In the case of 40039, thin section M40151B, however, there appear to be probably localised phosphate concentrations, staining the sediment matrix and infilling voids with Fe-P (see Fig. 5.13e; f). Finely punctuated iron nodules in essentially the same layer (see Fig. 5.3a; Fig. 5.13g; h; Fig. 5.4a) are also enriched in phosphate (eg 1.07%P). It is possible here that iron and phosphate are replacing amorphous organic matter, and that these are not simply FeP migration features, but related to localised inputs of organic matter and phosphate, as faecal waste (cf. Fe-P enriched Unit 4u at the Boxgrove Q1B waterhole site, associated with likely animal trampling, Macphail *et al.* 2001). At a butchery site perhaps animal remains are also a possibility. Associated textural pedofeatures that are indicative of physical mixing of wet sediments at context 40039, may tentatively suggest that phosphate and once-organic inputs are broadly related to large animal activity (see below).

Phase 1 deposits ('Tilted Block')

Context 40057 alluvium (coarse silts, fine sands) is characterised by the inclusion of moderately fresh glauconite (Loveland and Findlay 1982), suggesting inclusion of Tertiary sediments. Although weathered glauconite is present throughout the sediments above, fresh glauconite was little in evidence, indicating a change in provenance for Units Phases 6 and 6a, for example.

Phases 6 and 6a

Sediments, soils and vegetation

Sediments are often clayey, but may contain silts and fine sands at times. As noted above, they are strongly characterised by iron depletion and related iron panning and mottling, including the ferruginisation of roots. Clayey laminae can be interdigitated in sands as in the middle part of context 40039 (thin section M40323B, Fig. 5.10), suggesting seasonal variations in sedimentation, while in some coarse silty-fine sandy facies (for example, the upper part of context 40039, thin section M40323A, Fig. 5.11) very thin seasonal peat growth is perhaps recorded as ferruginised laminae (see also Fig. 5.18a; b). Fragments of iron-depleted clay in the same context, eroded from earlier-deposited clays, testify to sediment exposure and erosion related to renewed fluvial activity. It is also possible that cool climate erosion and colluvial processes could be involved, as in Unit 6a at Boxgrove (Macphail *et al.* 2001).

In addition to these variations in sedimentation, ephemeral sediment ripening took place (Avery 1990), when it was seasonally exposed to subaerial weathering. Plant growth is also recorded, and may have involved monocotyledonous wetland plants (see Fig. 5.13a; b; Fig 5.19a-d) and hence the sediment phytolith content, and later rooting by trees (see Fig. 5.13c; d), speculatively in a form of a hydroseral succession (Rodwell 1991) (cf. Pilgrim's School, Winchester, Macphail *et al.* 2009). Pollen evidence of woodland was previously noted (Wenban-Smith *et al.* 2006). The activity of rooting is one mechanism for mixing silts and sand into clayey sediments, alongside localised formation of textural pedofeatures associated with rooting into water-saturated sediments.

There is evidence of soil formation, which is presumably associated with this suggested hydroseral succession, such as in context 40103 (M40150A) and which is now seen as an 'ironpan' (see Fig. 5.3b, Fig. 5.16a-d and Fig. 5.4b). Differentially iron-stained soil and once organic materials are evidence of soil structure formation, activity by small invertebrate mesofauna and roots. When this soil was buried by renewed clayey alluviation (context 40099), the buried soil lost structure (becoming slaked), as is typical of inundated soils (cf. Unit 4c at Boxgrove).

Hominid and large animal activity

It is quite clear that inclusions and microfeatures associated with the presumed presence of hominids and other large animals are reflected in features of the soil-sediments. For example, putative artefacts (flint chips in the size range 4-20mm) occur as embedded clasts in muddy sediments and sediment clay is oriented around them; these small artefacts thus probably sank into the sediments (Fig. 5.10c; d; Fig. 5.16e; f; Fig. 5.17a; b) along with any other heavy objects. In addition, the amount of textural pedofeatures (clayey intercalations, void coatings) and associated closed vughs, infer more marked physical disturbance of water-saturated sediments than can be simply explained by rooting turbation (see above); large animal (and possibly also hominin) trampling may need to be envisaged. Equally, the presence of angular flint chips is anomalous in clayey sediments, and is best interpreted as related to anthropogenic activity.

Even though there are possible traces of rubefication and calcination, suggestive of burning, the latter most likely merely reflects patination and staining as typical fire-cracking is not in evidence (see Fig. 5.7a; b; Fig. 5.9c-e). There does, however, appear to be traces of what may be red burnt clay in the same context (40100; see Fig. 5.9a; b) and regular occurrences of burnt mineral grains. Charcoal is also found in the sediments (Fig. 5.13a; b; Fig. 5.19d). There are therefore weak but consistent indications of fire, but it remains to be established whether this may be derived from Tertiary sediments, or, if regarded as contemporary, whether it is merely natural wildfires periodically occurring, or whether of hominin origin. No hearth layers or other evidence of specifically hominin fire use were noted. Finally, the presence of sediments showing turbation, localised concentrations of relict organic matter and phosphate in the Phase 6 sediments in the vicinity of the elephant skeleton, and the associated flint artefact concentrations (thin sections M40365A, B and C; thin sections M40149 and M40150B) is unlikely to be a coincidence. As well as reflecting the more peaty organic-rich sediments associated with preservation of the skeleton, these characteristics may reflect hominin movement around the elephant skeleton, decay products of the elephant carcass and/or the presence of other living animals in the soft, waterlogged sediments around the elephant.

CONCLUSIONS

Nineteen thin sections (sediment micromorphology and SEM/EDS), 12 associated bulk samples (LOI and P) and 105 further bulk samples (LOI and magnetic susceptibility) were analysed, mostly from Phase 6, the main level of archaeological interest. Deposit formation processes included penecontemporaneous and post-depositional iron-depletion, organic matter oxidation, and iron and phosphate migration. Clayey and coarse silt-fine sandy alluvial and wetland sediments are present, and show probable seasonal variations in sedimentation and thin peat formation, for example. Ephemeral and longer lived sub-aerial weathering and soil formation is in evidence, including possible hydroseral succession(s) from, speculatively, monocotyledonous wetland to woodland and associated topsoil formation. Processes related to water table fluctuations, such as renewed alluviation and site inundation, are recorded generally. Hominid and large animal activity is probably recognisable from water-saturated sediment mixing. Most lithological evidence of burning is most likely of derived Tertiary origin; likewise, pieces of charcoal in the sediments are probably the result of contemporary wildfires, although a hominin role cannot be ruled out. Lastly, the presence of a butchered elephant carcass and artefacts in association with sediments showing turbation and localised concentrations of relict organic matter and phosphate may not simply be a coincidence. These latter observations are most likely to represent hominin movement, and possibly other activity, in the vicinity of the elephant carcass.